Joint neutrino oscillation analysis from the T2K and NOvA experiments

https://doi.org/10.1038/s41586-025-09599-3

Received: 11 April 2025

Accepted: 5 September 2025

Published online: 22 October 2025

Open access



The landmark discovery that neutrinos have mass and can change type (or flavour) as they propagate—a process called neutrino oscillation¹⁻⁶—has opened up a rich array of theoretical and experimental questions being actively pursued today. Neutrino oscillation remains the most powerful experimental tool for addressing many of these questions, including whether neutrinos violate charge-parity (CP) symmetry, which has possible connections to the unexplained preponderance of matter over antimatter in the Universe⁷⁻¹¹. Oscillation measurements also probe the mass-squared differences between the different neutrino mass states (Δm^2), whether there are two light states and a heavier one (normal ordering) or vice versa (inverted ordering), and the structure of neutrino mass and flavour mixing¹². Here we carry out the first joint analysis of datasets from NOvA¹³ and T2K¹⁴, the two currently operating long-baseline neutrino oscillation experiments (hundreds of kilometres of neutrino travel distance), taking advantage of our complementary experimental designs and setting new constraints on several neutrino sector parameters. This analysis provides new precision on the Δm^2_{32} mass difference, finding 2.43 $^{+0.04}_{-0.03}\times 10^{-3}~\text{eV}^2$ in the normal ordering and $-2.48^{+0.03}_{-0.04} \times 10^{-3} \text{ eV}^2$ in the inverted ordering, as well as a 3σ interval on δ_{CP} of [-1.38 π , 0.30π] in the normal ordering and $[-0.92\pi, -0.04\pi]$ in the inverted ordering. The data show no strong preference for either mass ordering, but notably, if inverted ordering were assumed true within the three-flavour mixing model, then our results would provide evidence of CP symmetry violation in the lepton sector.

The standard model of particle physics, extended to include neutrino mass, describes three-flavour eigenstates of neutrinos (v_e, v_μ, v_τ) that are related to three mass eigenstates (v_1, v_2, v_3) by the 3×3 complex Pontecorvo–Maki–Nakagawa–Sakata unitary mixing matrix U_{PMNS} (refs. 15–17). This mixing, together with non-zero neutrino mass, allows for the phenomenon of neutrino oscillation, in which, during propagation, the flavour content of a neutrino evolves at a rate that depends on neutrino mass-squared splittings $(\Delta m_{ij}^2 \equiv m_i^2 - m_j^2)$ and the U_{PMNS} matrix elements. Apart from these oscillation parameters, the rate depends on neutrino energy E_ν and neutrino propagation distance L (baseline). Although experiments studying this process in recent decades have provided insights into the details of neutrino masses and mixings¹², many open questions remain.

The mixing matrix $U_{\rm PMNS}$ is typically parameterized in terms of three mixing angles $(\theta_{12},\theta_{13},\theta_{23})$ and at least one complex phase $\delta_{\rm CP}$ (ref. 12). It is unknown whether $\sin\delta_{\rm CP}$ is non-zero; if it is, neutrinos—and thus leptons—violate charge-parity (CP) symmetry and thereby provide a source of matter—antimatter asymmetry in nature 17, which is of great interest given the connection between CP violation and the unexplained matter dominance in the Universe 7-11. Separately, oscillation experiments have established that the mass-squared splitting Δm_{32}^2 is roughly 30 times larger in magnitude than Δm_{21}^2 , but the sign of the former is at present unknown. That is, v_3 may be heavier or lighter than the v_1-v_2 pair, with these two options termed, respectively, the normal $(\Delta m_{32}^2 > 0)$ and inverted $(\Delta m_{32}^2 < 0)$ mass orderings. Knowledge of the mass

ordering can constrain experimental searches and theory development in a wide range of physics, including absolute neutrino mass measurements¹⁸, neutrinoless double beta decay searches to investigate the nature of neutrino mass¹⁹, models of supernova explosion and detection^{20,21}, and the cosmological evolution evidenced in cosmic microwave background and large-scale structure measurements²². For the mixing angles, current data suggest θ_{23} is near 45°, a notable value hinting at a μ/τ flavour symmetry¹⁷. Improved precision on this and other mixing angles is essential for gaining a clearer view of flavour mixing and to probe the validity of the three-flavour model.

Long-baseline accelerator neutrino oscillation experiments are well suited to address the above questions. In these, a high-intensity neutrino beam enriched in muon neutrinos (ν_μ) or muon antineutrinos $(\overline{\nu}_\mu)$ is produced at a particle accelerator and directed through the crust of Earth towards a massive far detector located hundreds of kilometres away. Note that the word 'neutrino' is used to mean both neutrino and antineutrino unless stated otherwise. The far detector measures the event rates of ν_μ and ν_e —the latter primarily from $\nu_\mu \rightarrow \nu_e$ oscillation—as a function of neutrino energy, from which the oscillation parameters above can be determined. These experiments use near detectors, sited a short distance from the beam source, in which oscillation effects are negligible and a very high neutrino event rate can be measured. The near detectors provide vital control measurements that substantially mitigate large systematic uncertainties in the initial neutrino flux, neutrino-on-nucleus interaction cross-sections and in some cases

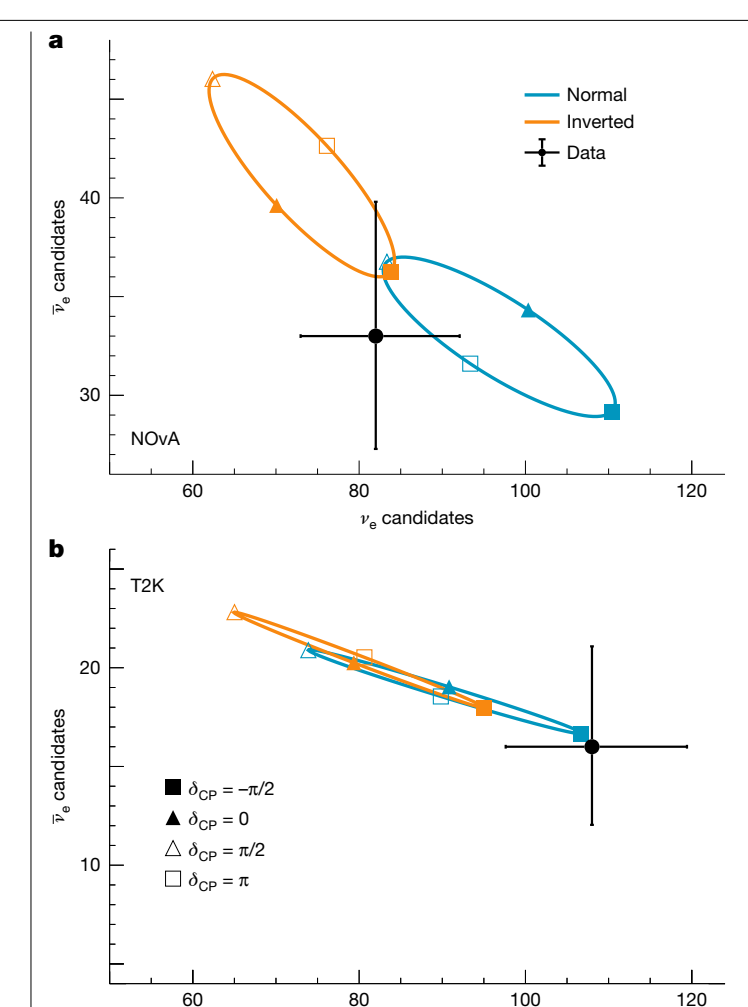


Fig. 1| The impact of mass ordering and δ_{CP} on event rates. a,b, A bi-event plot that shows experimental sensitivity to neutrino mass ordering and $\delta_{\rm CP}$, with panels representing the NOvA (a) and T2K (b) cases. Black points with 1σ Poisson statistical error bars show the total number of v_e and \overline{v}_e candidates selected in the far detectors. The oval parametric curves trace out predicted numbers of events under the normal (blue) or inverted (orange) mass ordering assumption as the parameter δ_{CP} varies from $-\pi$ to π . Four specific δ_{CP} values are labelled for reference. All other oscillation parameters are kept fixed in this graphic, set to their most probable values from the joint analysis (Extended Data Table 3).

 $\nu_{\rm e}$ candidates

detector response (for example, energy reconstruction and event selection efficiencies).

Two such experiments are in operation today, T2K and NOvA. Each experiment uses a narrow-band off-axis beam^{23,24}, whose peak energy is near the first oscillation maximum, $\sin^2\left(\frac{\Delta m_{32}^2 L}{4E}\right) \approx 1$, at the far detec-

tor. Note that natural units, where $\hbar = c = 1$, are used throughout. T2K uses an approximately 0.6 GeV neutrino beam from J-PARC in Tokai, Japan, and the 50-kt Super-Kamiokande water Cherenkov detector for its far detector located 295 km away²⁵. In the United States, an approximately 2 GeV beam of NOvA is produced at Fermilab near Chicago, and the 14-kt tracking calorimeter far detector is located 810 km away in northern Minnesota²⁶. Further details on the designs of NOvA and T2K and on long-baseline experiments can be found in the Methods and refs. 25-27.

We report here a combined analysis of the datasets from T2K and NOvA previously analysed independently in refs. 13,14. This combination takes advantage of marked complementarity in the sensitivities of the two experiments to the oscillation parameters. In particular,

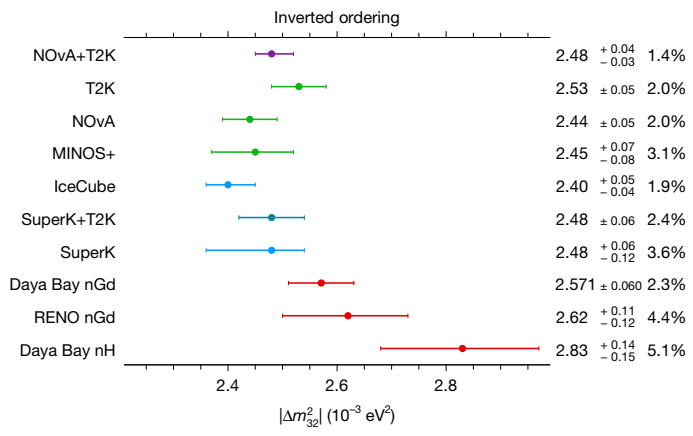


Fig. 2 | Experimental measurements of $|\Delta m_{32}^2|$. The measurements assume the inverted ordering preferred by this analysis. Sources for the results from top to bottom, starting with the second line, are as follows: refs. 13,14,43-49. The normal ordering case is available in Extended Data Fig. 9.

the $v_{\mu} \rightarrow v_{e}$ oscillation probability is a function of (among other things) both $\delta_{\rm CP}$ and the neutrino mass ordering, and these two effects must be teased apart.

Figure 1 shows the complementarity between the experiments in a simplified case. Sets of oval curves indicate the energy-integrated total v_a and \overline{v}_a event counts expected in the far detectors under various mass ordering and δ_{CP} scenarios, with other oscillation parameters held fixed. The measured event counts in NOvA and T2K are shown as black points with error bars.

As shown in Fig. 1a, there is stronger separation between the mass ordering ovals for NOvA, because of higher beam energies, but as the NOvA data lie near the overlap of the ellipses, there can be ambiguity as to which ordering is correct and (in a correlated way) which values of $\delta_{\rm CP}$ are preferred. By contrast, T2K has less sensitivity to the mass ordering, but points with similar values of δ_{CP} in each hierarchy sit close to one another, and the data lie closest to $\delta_{CP} = -\frac{\pi}{2}$, regardless of mass ordering. Combining these datasets can provide simultaneous mass ordering and δ_{CP} information with substantially less ambiguity, maximizing the use of current data and informing data-taking strategies for current and future experiments.

This discussion points to a more general observation that the oscillation parameters of interest represent a highly correlated multidimensional space. The analysis reported here calculates a joint Bayesian posterior, using the likelihoods of the experiments defined over the full parameter space. Moreover, we use the full suite of analysis tools from both experiments: detector response models, neutrino energy estimators, near-detector measurements and systematic uncertainties, all within a unified framework for statistical inference. This level of integration is the first for accelerator neutrino experiments, to our knowledge.

The posterior calculation is based on detailed parameterized models of the neutrino flux, cross-sections and detectors that predict the binned spectra of neutrino events in each of our selected samples as a function of the oscillation parameters and a large number of nuisance parameters mostly related to systematic uncertainties in the models. A likelihood is constructed from Poisson probability terms describing the compatibility between the prediction and the observed data in bins of relevant variables. Prior probabilities are set on all parameters as detailed in the Methods.

Both T2K and NOvA have software that explores the posterior using Markov chain Monte Carlo (MCMC) methods^{28,29} (ARIA for NOvA³⁰ and MaCh3 for T2K³¹). By containerizing³² the likelihood and prior portions of the code, we can construct and analyse the joint posterior using either of the original MCMC frameworks, in spite of the very different

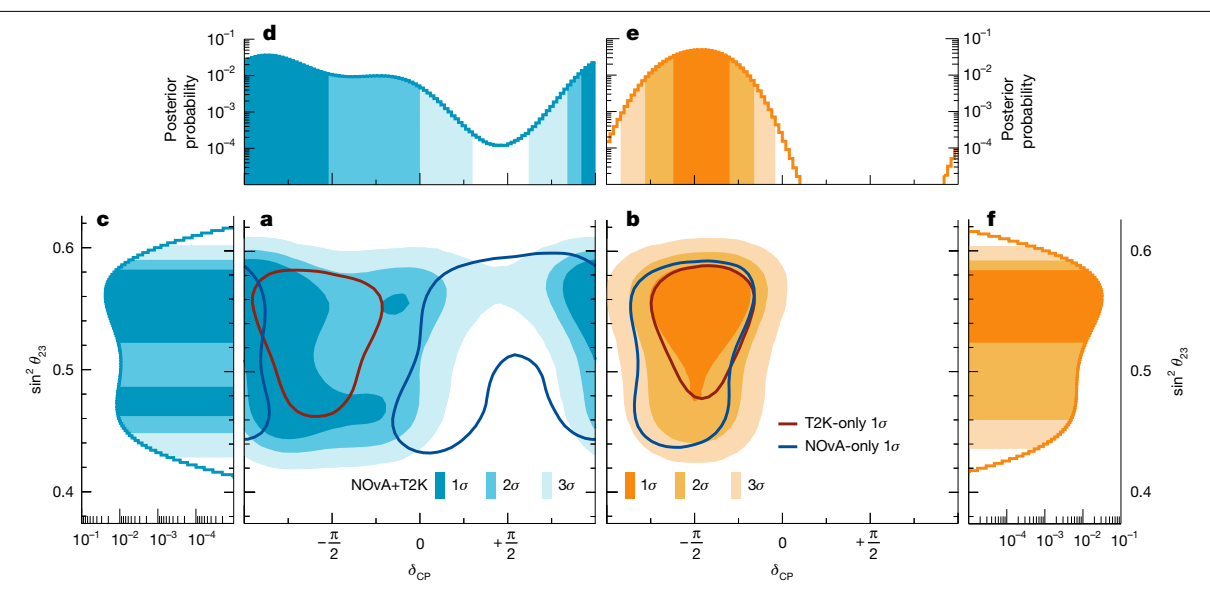


Fig. 3 | **Constraints on \sin^2\theta_{23} and \delta_{\text{CP}}.** Marginalized posterior probabilities and 1D or 2D Bayesian credible regions of $\sin^2\theta_{23}$ and δ_{CP} in the case of the normal (blue, left side) and inverted (orange, right side) neutrino mass ordering with the reactor constraint applied. Shaded areas correspond to 1σ , 2σ and 3σ credible regions. **a,b**, The 2D panels of $\sin^2\theta_{23}$ vs δ_{CP} (**a,b**) are overlaid with 1σ

credible regions from the T2K-only (dark red) and NOvA-only (dark blue) data fits assuming normal (**a**) and inverted ordering (**b**). **c**–**f**, The 1D panels show the posterior probabilities of $\sin^2\theta_{23}$ (**c**) and $\delta_{\rm CP}$ (**d**) in the normal ordering, and $\delta_{\rm CP}$ (**e**) and $\sin^2\theta_{23}$ (**f**) in the inverted ordering.

software environments involved. For each fitting framework, ARIA or MaCh3, the native likelihood and priors of the fitter are calculated directly, whereas the likelihood and priors of other experiments are accessed using the software container. In this way, either framework can be used, providing valuable redundancy and thus cross-checks of all statistical inferences.

Although a single set of oscillation parameters naturally applies to both experiments in the joint posterior, the treatment of the many nuisance parameters related to systematic uncertainties is more subtle. Both measurements of the oscillation parameters at present have statistical uncertainties larger than the systematic uncertainties, but the latter are not negligible. We thoroughly surveyed the flux, cross-section and detector models and their systematic uncertainties to determine whether correlations between the experiments affect the analysis at a significant level. Our conclusions from this effort are summarized in the following paragraphs.

Both T2K and NOvA use beams produced by directing accelerated protons onto graphite targets. The hadrons are charge-selected with magnetic horns: positively charged hadrons decay to produce neutrinos, and negatively charged hadrons produce antineutrinos. Many uncertainties on these beam fluxes stem from processes unrelated between the two experiments, for example, the alignment of beam components. Yet, uncertainties on the rate of hadron production in the graphite targets are substantial, and the underlying physics is the same. However, the two experiments use proton beams of different energies (30 GeV for T2K and 120 GeV for NOvA), and the external datasets used to tune the hadron production models of both experiments are different³³⁻³⁵. Moreover, the ultimate impact of flux uncertainties on far-detector predictions in NOvA is much smaller than other uncertainties. We, therefore, conclude that at current experimental exposures, the flux uncertainties of the two experiments need not be correlated.

Given the different detector technologies involved, most detector-related uncertainties are independent between the experiments. Furthermore, the very different energy estimation techniques used, combined with model tuning and uncertainty estimation using in situ calibration samples in each experiment, including for the lepton and neutron energy scales, lead to independence between the two detector

uncertainty models. We conclude that there are no significant correlations in the detector models.

For neutrino-on-nucleus cross-sections, the underlying physics is the same; in many cases, the same external datasets are used by both experiments to tune and set prior uncertainties on model parameters. Thus, cross-section model correlations are expected. However, in the specific case of NOvA and T2K, the description of this physics differs markedly. The simulation packages differ 36,37, the physical models implemented in them differ in many places, the parameterizations differ almost entirely, and customized tunings are necessary and applied, given the specific energies of the experiments, detector technologies and approaches to systematic uncertainty mitigation.

Proper correlations between experiments could be implemented by starting from a common cross-section model spanning different energy ranges and able to describe both the leptonic and hadronic parts of the final state. A joint description is not yet mature and is one of the focuses of the community in the years to come³⁸. Given the differences in the models, a direct mapping of their parameters was deemed not practical at this time. Instead, we studied whether neglecting these correlations could appreciably affect our measurements of the oscillation parameters. The studies are limited to our current experimental exposures and models and would need re-evaluation if applied to any other context.

First, we assessed whether correlations between single systematic parameters in our models could have a substantial impact on our results. For each of Δm_{32}^2 , θ_{23} and $\delta_{\rm CP}$, we identified the systematic parameter in each experiment with the largest impact on the measurement of that oscillation parameter. Then, regardless of whether those two systematic parameters made physical sense to correlate, we performed fits to simulated pseudo-data with the parameters fully correlated, uncorrelated and fully anticorrelated. Details of these studies, including how we identified the most impactful parameters, are shown in the Methods. In summary, we saw no case in which the choice of correlation of individual systematic parameters significantly affected the oscillation parameter measurements.

Checking individual parameters does not rule out effects from a mix of systematic parameter variations that combine to produce a net effect that is larger and possibly more degenerate with oscillation

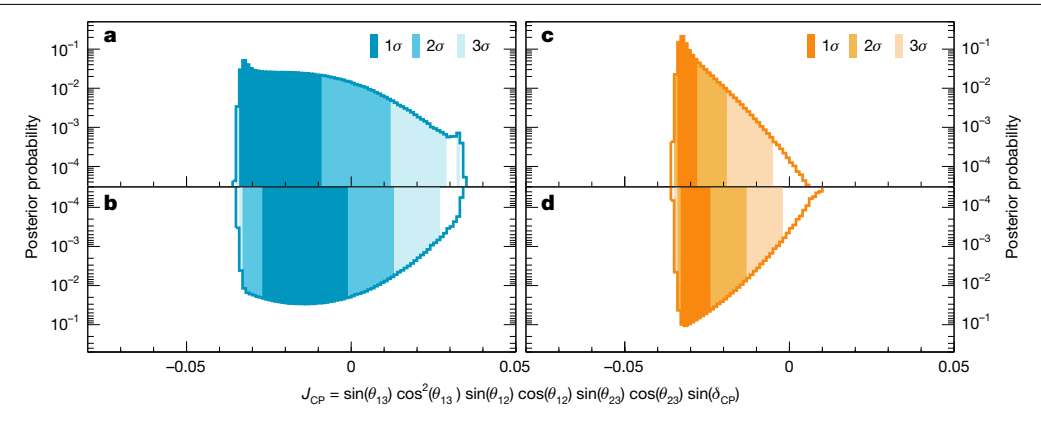


Fig. 4 | Constraints on the Jarlskog invariant. a-d, Marginalized posterior probabilities of the Jarlskog invariant, J_{CP} , in the case of the normal (blue; \mathbf{a} , \mathbf{b}) and inverted (orange; **c**,**d**) neutrino mass ordering with the reactor constraint

applied. The posterior distributions use prior distributions either flat in $\delta_{CP}(\mathbf{a},\mathbf{c})$ or $\sin \delta_{CP}(\mathbf{b},\mathbf{d})$. Shaded areas show the 1σ , 2σ and 3σ Bayesian credible intervals

effects, representing a potential worst-case scenario for the analyses. Rather than seeking such a set of variations, we directly identified, or in some cases constructed, single systematic parameters for each experiment that have effects similar to each oscillation parameter of interest. We then adjusted the size of the priors on these 'nightmare' parameters such that their impact on the measurements is comparable to that of statistical errors and therefore larger than the net effect of all our regular systematic parameters combined. These nightmare parameters were added to our nominal uncertainty models to create augmented models, allowing us to study a case in which systematic effects are comparable to statistical uncertainty. Next, we constructed simulated pseudo-datasets with the nightmare parameters increased in both experiments by one standard deviation above their prior central values. These simulated pseudo-data were then fit three times using the augmented model: once with the nightmare parameters of the experiments fully correlated (matching the pseudo-data), once fully anticorrelated and finally uncorrelated. We find that the oscillation parameter constraints extracted in the fully correlated and uncorrelated cases have negligible differences. However, the incorrect anticorrelated case yields a large bias. We expect that with even larger systematic uncertainties, differences between the correlated and uncorrelated cases would eventually become relevant. However, this study indicates that we are not in such a regime with the current exposures and systematic uncertainties (see the Methods for further results).

Given that no significant biases are seen from neglecting correlations between actual systematic parameters, and the only bias seen with the nightmare parameters comes not from neglecting a correlation but from adding an incorrect one, we choose in most cases to neglect the correlations between the systematic uncertainties of the two experiments. The one exception relates to the approximately 2% normalization uncertainties on all v_e and $\overline{v_e}$ events described in ref. 39. In this case, the uncertainties are implemented identically by T2K and NOvA, and we have correlated them.

We also perform studies in which the joint fit is tested against pseudodata constructed with a set of discrete model variations not directly accessible using the nominal uncertainty models of the experiments. This procedure was used in the earlier independent T2K analysis¹⁴, and we include in the present analysis those model variations seen as most impactful previously. Similarly, we studied a secondary set of variations based on extrapolating the cross-section model of each experiment to the context of the other experiment. Predefined thresholds were used to establish that no substantive changes in the central values or interval widths of the oscillation parameters were seen under these tests, as described in the Methods. For all tested alternative models, all observed changes in credible intervals were within thresholds (see the Methods for further details). Each experiment continues to investigate improvements in its cross-section models, and the studies described here would warrant repeating for larger data exposures and/or updated theoretical understanding. Continued theoretical and experimental effort in this direction is important.

With the joint likelihood and systematic uncertainty model defined, we use our fitting frameworks to analyse the combined datasets of refs. 13,14, finding consistent results between the two frameworks. Unless stated otherwise, we report results using an external constraint on θ_{13} (named the 'reactor constraint' below) and external constraints on Δm_{21}^2 and θ_{12} . The values used for these constraints correspond to the 2020 Particle Data Group summary values⁴⁰ and are given in the Methods

We tested the goodness of fit (Methods) of our model to data using the P-value method⁴¹, both overall and for each individual sample in the far detectors. All the P-values are within an acceptable range (>0.05 after the look-elsewhere-effect adjustment described in the Methods). The overall P-value to describe all NOvA and T2K samples is 0.75 for full spectral analysis and 0.40 for rate-only analysis, marginalized over both mass orderings. Similar results were obtained without the reactor constraint and in each mass ordering. Thus, the joint oscillation model simultaneously fits T2K and NOvA data well. The P-values are also consistent with those of previous T2K-only and NOvA-only analyses.

We produce parameter estimations using the highest-posteriordensity credible intervals and perform discrete hypothesis tests using the Bayes factor formalism. Conclusions related to CP conservation or violation, Δm_{32}^2 , $\sin^2\theta_{23}$ and mass ordering have been tested to be robust under the alternative model variations described previously. For the measured oscillation parameters, we report 1σ (68.27%) credible intervals unless noted.

We find $\sin^2\!\theta_{23} = 0.56^{+0.03}_{-0.05}$ without any assumptions on the ordering of the neutrino masses. The fit weakly prefers the upper octant of θ_{23} $(\sin^2\theta_{23} > 0.5)$ over the lower octant with a Bayes factor of 3.5. Removing the reactor constraint gives no statistically significant preference for either octant (Bayes factor 1.2 for the lower octant compared with the upper octant). We also find $\Delta m_{32}^2 = 2.43^{+0.04}_{-0.03} \times 10^{-3} \ {\rm eV^2}$ assuming the normal ordering and $\Delta m_{32}^2 = -2.48^{+0.03}_{-0.04} \times 10^{-3} \ {\rm eV^2}$ assuming the inverted ordering. This is at present the smallest experimental uncertainty on $|\Delta m_{32}^2|$ (Fig. 2), to our knowledge. This conclusion also applies when the reactor constraint is replaced by a flat prior.

There is no statistically significant preference obtained for either of the mass orderings, with a Bayes factor of 1.3 in favour of the inverted ordering with reactor θ_{13} constraint and 2.5 without reactor θ_{13} constraint. Although the two experiments individually prefer the normal ordering, the values of other oscillation parameters are more consistent in the inverted ordering, leading to a different ordering preference in the joint fit, although still not statistically significant. The effect on

mass ordering preference when additionally incorporating reactor Δm_{32}^2 measurements is discussed in the Methods.

With no assumption on the true mass ordering, we find the 1σ credible interval on δ_{CP} to contain $[-0.81\pi, -0.26\pi]$ with the highest posterior probability value being -0.47π . We also find that values of δ_{CP} around $+\pi/2$, an extremum of $\sin \delta_{CP}$, are outside our 3σ (99.73%) credible intervals, which also holds for either mass ordering separately. Figure 3 shows the joint fit result compared with the individual measurements of NOvA and T2K in the $\sin^2\theta_{23} - \delta_{CP}$ plane, as well as onedimensional (1D) uniformly binned posterior probability distributions for both mass ordering cases. Assuming the normal ordering, the joint analysis allows a wide range of δ_{CP} values, giving a 3σ credible interval of $\delta_{CP} \in [-1.38\pi, 0.30\pi]$. In the case of the inverted ordering $\delta_{CP} \in [-0.92\pi, -0.04\pi]$, excluding 56% of the parameter space, the CP-conserving values of $\delta_{CP} = 0$ and π are outside the 3σ credible interval. A consistent picture is seen when analysing the Jarlskog invariant, J_{CP} (ref. 42), which is a parametrization-independent measure of CP violation. The CP-conserving value of $J_{CP} = 0$ falls outside the 3σ credible interval for the inverted ordering, and the above statements are true whether the prior used is uniform in δ_{CP} or $\sin \delta_{CP}$ (Fig. 4). This analysis, therefore, provides evidence for CP violation in the lepton sector if the inverted ordering is assumed to be true. However, we do not see a significant preference at present for either mass ordering. Future mass ordering measurements will, therefore, influence the interpretation of these results. See the Methods for more data projections and comparisons.

Online content

Any methods, additional references, Nature Portfolio reporting summaries, source data, extended data, supplementary information, acknowledgements, peer review information; details of author contributions and competing interests; and statements of data and code availability are available at https://doi.org/10.1038/s41586-025-09599-3.

- Fukuda, Y. et al. Evidence for oscillation of atmospheric neutrinos. *Phys. Rev. Lett.* 81, 1562–1567 (1998).
 Fukuda, S. et al. Determination of solar neutrino oscillation parameters using 1496 days of
- Super-Kamiokande-I data. *Phys. Lett. B* **539**, 179–187 (2002).

 3. Ahmad, Q. R. et al. Measurement of the rate of $v_a + d \rightarrow p + p + e^-$ interactions produced by
- Ahmad, Q. R. et al. Measurement of the rate of v_e+d→p+p+e⁻ interactions produced by ⁸B solar neutrinos at the Sudbury Neutrino Observatory. Phys. Rev. Lett. 87, 071301 (2001).
- Ahmad, Q. R. et al. Direct evidence for neutrino flavor transformation from neutral-current interactions in the Sudbury Neutrino Observatory. Phys. Rev. Lett. 89, 011301 (2002).
- Eguchi, K. et al. First results from KamLAND: evidence for reactor antineutrino disappearance. Phys. Rev. Lett. 90, 021802 (2003).
- An, F. P. et al. Observation of electron-antineutrino disappearance at Daya Bay. Phys. Rev. Lett. 108, 171803 (2012).
- Fukugita, M. & Yanagida, T. Barygenesis without grand unification. Phys. Lett. B 174, 45–47 (1986)
- Buchmüller, W., Peccei, R. D. & Yanagida, T. Leptogenesis as the origin of matter. Annu. Rev. Nucl. Part. Sci. 55, 311–355 (2005).
- Pascoli, S., Petcov, S. T. & Riotto, A. Connecting low energy leptonic CP violation to leptogenesis. Phys. Rev. D 75, 083511 (2007).
- Branco, G. C., Gonzalez Felipe, R. & Joaquim, F. R. Leptonic CP violation. Rev. Mod. Phys. 84, 515–565 (2012).
- Hagedorn, C., Mohapatra, R. N., Molinaro, E., Nishi, C. C. & Petcov, S. T. CP violation in the lepton sector and implications for leptogenesis. *Int. J. Mod. Phys. A* 33, 1842006 (2018).
- Particle Data Group et al. Review of particle physics. Prog. Theor. Exp. Phys. 2022, 083C01 (2022).
- Acero, M. A. et al. Improved measurement of neutrino oscillation parameters by the NOvA experiment. Phys. Rev. D 106, 032004 (2022).
- Abe, K. et al. Measurements of neutrino oscillation parameters from the T2K experiment using 3.6×10²¹ protons on target. Eur. Phys. J. C 83, 782 (2023).
- Maki, Z., Nakagawa, M. & Sakata, S. Remarks on the unified model of elementary particles Prog. Theor. Phys. 28, 870–880 (1962).
- Pontecorvo, B. Neutrino experiments and the problem of conservation of leptonic charge. Zh. Eksp. Teor. Fiz. 53, 1717–1725 (1967).
- 17. Mohapatra, R. N. et al. Theory of neutrinos: a white paper. Rep. Prog. Phys. 70, 1757 (2007).
- Formaggio, J. A., de Gouvea, A. L. C. & Robertson, R. G. H. Direct measurements of neutrino mass. Phys. Rep. 914, 1–54 (2021).
- Dolinski, M. J., Poon, A. W. P. & Rodejohann, W. Neutrinoless double-beta decay: status and prospects. *Annu. Rev. Nucl. Part. Sci.* 69, 219–251 (2019).
- Hansen, R. S. L., Lindner, M. & Scholer, O. Timing the neutrino signal of a galactic supernova. Phys. Rev. D 101, 123018 (2020).

- Horiuchi, S. & Kneller, J. P. What can be learned from a future supernova neutrino detection? J. Phys. G 45, 043002 (2018).
- Lesgourgues, J. & Pastor, S. Neutrino mass from cosmology. Adv. High Energy Phys. 2012, 608515 (2012).
- Beavis, D., Carroll, A. & Chiang, I. Long Baseline Neutrino Oscillation Experiment at the AGS. Physics Design Report. Report No. 52459 (Brookhaven National Laboratory, 1995).
- Helmer, R. L. A new long baseline neutrino oscillation experiment at Brookhaven. In Proc. 9th Lake Louise Winter Institute: Particle Physics and Cosmology (LLWI 1994) 291–301 (1994)
- Abe, K. et al. The T2K experiment. Nucl. Instrum. Methods Phys. Res. A 659, 106–135 (2011).
- Ayres, D. S. et al. The NOvA Technical Design Report. Report No. FERMILAB-DESIGN-2007-01 (Fermilab National Accelerator Laboratory, 2007).
- Di Lodovico, F., Patterson, R. B., Shiozawa, M. & Worcester, E. Experimental considerations in long-baseline neutrino oscillation measurements. *Annu. Rev. Nucl. Part. Sci.* 73, 69–93 (2023).
- Metropolis, N., Rosenbluth, A. W., Rosenbluth, M. N., Teller, A. H. & Teller, E. Equation of state calculations by fast computing machines. J. Chem. Phys. 21, 1087–1092 (1953).
- Hastings, W. K. Monte Carlo sampling methods using Markov chains and their applications. *Biometrika* 57, 97-109 (1970).
- Acero, M. A. et al. Expanding neutrino oscillation parameter measurements in NOvA using a Bayesian approach. Phys. Rev. D 110, 012005 (2024).
- The MaCh3 Collaboration. mach3-software/MaCh3: v1.5.0 (v1.5.0). Zenodo https://doi. org/10.5281/zenodo.15319160 (2024).
- Kurtzer, G. M., Sochat, V. & Bauer, M. W. Singularity: scientific containers for mobility of compute. PloS One 12, e0177459 (2017).
- Alt, C. et al. Inclusive production of charged pions in p+C collisions at 158 GeV/c beam momentum. Eur. Phys. J. C 49, 897–917 (2007).
- Abgrall, N. et al. Measurements of π^{*} differential yields from the surface of the T2K replica target for incoming 31 GeV/c protons with the NA61/SHINE spectrometer at the CERN SPS. Eur. Phys. J. C 76, 617 (2016).
- 35. Abgrall, N. et al. Measurements of π^{\pm} , K_S^0 , Λ and proton production in proton–carbon interactions at 31 GeV/c with the NA61/SHINE spectrometer at the CERN SPS. *Eur. Phys. J.*
- Hayato, Y. & Pickering, L. The NEUT neutrino interaction simulation program library. Eur. Phys. J. Spec. Top. 230, 4469–4481 (2021).
- Andreopoulos, C. et al. The GENIE neutrino Monte Carlo generator. Nucl. Instrum. Methods Phys. Rev. A 614, 87-104 (2010).
- Balantekin, A. B. et al. Snowmass Neutrino Frontier: Neutrino Interaction Cross Sections (NF06) Topical Group Report. Preprint at arxiv.org/abs/2209.06872 (2022).
- Day, M. & McFarland, K. S. Differences in quasielastic cross sections of muon and electron neutrinos. Phys. Rev. D 86, 053003 (2012).
- 40. Zyla, P. A. et al. Review of particle physics. Prog. Theor. Exp. Phys. 2020, 083C01 (2020).
- Gelman, A., Meng, X. & Stern, H. Posterior predictive assessment of model fitness via realized discrepancies. Stat. Sin. 6, 733–760 (1996).
- Jarlskog, C. A basis independent formulation of the connection between quark mass matrices, CP violation and experiment. Z. Phys. C Part. Fields 29, 491–497 (1985).
- Adamson, P. et al. Precision constraints for three-flavor neutrino oscillations from the full MINOS+ and MINOS dataset. Phys. Rev. Lett. 125, 131802 (2020).
- Abbasi, R. et al. Measurement of atmospheric neutrino oscillation parameters using convolutional neural networks with 9.3 years of data in IceCube DeepCore. Phys. Rev. Lett. 134, 091801 (2025).
- Abe, K. et al. First joint oscillation analysis of Super-Kamiokande atmospheric and T2K accelerator neutrino data. Phys. Rev. Lett. 134, 011801 (2025).
- 46. Wester, T. et al. Atmospheric neutrino oscillation analysis with neutron tagging and an expanded fiducial volume in Super-Kamiokande I-V. Phys. Rev. D **109**, 072014 (2024).
- An, F. P. et al. Precision measurement of reactor antineutrino oscillation at kilometer-scale baselines by Daya Bay. Phys. Rev. Lett. 130, 161802 (2023).
- Jeon, S. et al. Measurement of reactor antineutrino oscillation parameters using the full 3800-day dataset of the RENO experiment. Phys. Rev. D 111, 112006 (2025).
- An, F. P. et al. Measurement of electron antineutrino oscillation amplitude and frequency via neutron capture on hydrogen at Daya Bay. Phys. Rev. Lett. 133, 151801 (2024).

 $\textbf{Publisher's note} \ Springer \ Nature \ remains \ neutral \ with \ regard \ to \ jurisdictional \ claims \ in \ published \ maps \ and \ institutional \ affiliations.$



Open Access This article is licensed under a Creative Commons Attribution 4.0 International License, which permits use, sharing, adaptation, distribution and reproduction in any medium or format, as long as you give appropriate

credit to the original author(s) and the source, provide a link to the Creative Commons licence, and indicate if changes were made. The images or other third party material in this article are included in the article's Creative Commons licence, unless indicated otherwise in a credit line to the material. If material is not included in the article's Creative Commons licence and your intended use is not permitted by statutory regulation or exceeds the permitted use, you will need to obtain permission directly from the copyright holder. To view a copy of this licence, visit http://creativecommons.org/licenses/by/4.0/.

© The Author(s) 2025

The NOvA Collaboration

S. Abubakar¹, M. A. Acero², B. Acharya³, P. Adamson⁴, N. Anfimov⁵, A. Antoshkin⁵, E. Arrieta-Diaz⁶, L. Asquith⁷, A. Aurisano⁸, D. Azevedo⁹, A. Back^{10,1}, N. Balashov⁵, P. Baldi¹², B. A. Bambah¹³, E. F. Bannister⁷, A. Barros², A. Bat¹⁴, K. Bays¹⁵, R. Bernstein⁴, T. J. C. Bezerra⁷, V. Bhatnagar¹⁶, B. Bhuyan¹⁷, J. Bian^{12,15}, A. C. Booth^{7,16}, R. Bowles¹⁰, B. Brahma¹⁹, C. Bromberg²⁰, N. Buchanan²¹, A. Butkevich²², S. Calvez²¹, J. M. Carceller²³, T. J. Carroll^{24,25},

E. Catano-Mur²⁶, J. P. Cesar²⁴, R. Chirco²⁷, B. C. Choudhary²⁸, A. Christensen²¹, M. F. Cicala²³, T. E. Coan²⁹, T. Contreras⁴, A. Cooleybeck²⁵, D. Coveyou³⁰, L. Cremonesi¹⁸, G. S. Davies³, P. F. Derwent⁴, P. Ding⁴, Z. Djurcic³¹, K. Dobbs³², M. Dolce³³, D. Dueñas Tonguino⁸, E. C. Dukes³⁰, A. Dye³, R. Ehrlich³⁰, E. Ewart¹⁰, P. Filip³⁴, M. J. Frank³⁵, H. R. Gallagher³⁶, A. Giri¹⁹, R. A. Gomes⁹, M. C. Goodman³¹, R. Group³⁰, A. Habig³⁷, F. Hakl³⁸, J. Hartnell⁷, R. Hatcher⁴, J. M. Hays¹⁸, M. He³², K. Heller¹⁵, V. Hewes⁸, A. Himmel⁴, T. Horoho³⁰ A. Ivanova⁵, B. Jargowsky¹², I. Kakorin⁵, A. Kalitkina⁵, D. M. Kaplan²⁷, A. Khanam³⁹, B. Kirezli¹, J. Kleykamp³, O. Klimov⁵, L. W. Koerner³², L. Kolupaeva⁵, R. Kralik⁷, A. Kumar¹⁶, C. D. Kuruppu⁴⁰, V. Kus⁴¹, T. Lackey^{4,10}, K. Lang²⁴, P. Lasorak⁷, J. Lesmeister³², A. Lister²⁵, J. Liu¹², J. A. Lock⁷, M. MacMahon²³, S. Magill³¹, W. A. Mann³⁶, M. T. Manoharan M. Manrique Plata¹⁰, M. L. Marshak¹⁵, M. Martinez-Casales^{4,11}, V. Matveev²², B. Mehta¹⁶, M. D. Messier¹⁰, H. Meyer³³, T. Miao⁴, W. H. Miller¹⁵, S. R. Mishra⁴⁰, R. Mohanta¹³, A. Moren³⁷, A. Morozova⁵, W. Mu⁴, L. Mualem⁴³, M. Muether³³, K. Mulder²³, D. Myers²⁴, D. Naples⁴⁴, S. Nelleri⁴², J. K. Nelson²⁶, R. Nichol²³, E. Niner⁴, A. Norman⁴, A. Norrick⁴, H. Oh⁸, A. Olshevskiy⁵, T. Olson³², M. Ozkaynak²³, A. Pal⁴⁵, J. Paley⁴, L. Panda⁴⁵, R. B. Patterson⁴³, G. Pawloski¹⁵, R. Petti⁴⁰, R. K. Plunkett⁴, J. C. C. Porter⁷, L. R. Prais^{3,8}, A. Rafique³¹, V. Raj⁴³, M. Rajaoalisoa⁸, B. Ramson⁴, B. Rebel²⁵, E. Robles¹², P. Roy³³, O. Samoylov⁵, M. C. Sanchez^{11,46}, S. Sánchez Falero¹¹, P. Shanahan⁴, P. Sharma¹⁶, A. Sheshukov⁵, Shiyam¹⁷, A. Shmakov¹², W. Shorrock⁷, S. Shukla⁴⁷, I. Singh²⁸, P. Singh^{18,28}, V. Singh⁴⁷, S. Singh Chhibra¹⁸, D. K. Singha¹³, A. Smith¹⁵, J. Smolik⁴¹, P. Snopok²⁷, N. Solomey³³, A. Sousa⁸, K. Soustruznik⁴⁸, M. Strait^{4,15}, L. Suter⁴, A. Sutton^{11,46}, S. Swain⁴⁵, C. Sweeney²³, A. Sztuc²³, N. Talukdar⁴⁰, P. Tas⁴⁸, T. Thakore⁸, J. Thomas²³, E. Tiras^{1,11}, M. Titus⁴², Y. Torun²⁷, D. Tran³ J. Trokan-Tenorio²⁶, J. Urheim¹⁰, P. Vahle²⁶, Z. Vallari⁴⁹, K. J. Vockerodt¹⁸, A. V. Waldron¹⁸, M. Wallbank^{4,8}, T. K. Warburton¹¹, C. Weber¹⁵, M. Wetstein¹¹, D. Whittington^{10,38} D. A. Wickremasinghe⁴, J. Wolcott³⁶, S. Wu¹⁵, W. Wu¹², W. Wu⁴⁴, Y. Xiao¹², B. Yaeggy⁸, A. Yahaya³³, A. Yankelevich¹², K. Yonehara⁴, S. Zadorozhnyy²², J. Zalesak³⁴ & R. Zwaska⁴

¹Department of Physics, Erciyes University, Kayseri, Turkey. ²Universidad del Atlantico, Puerto Colombia, Colombia. 3University of Mississippi, Lafayette, MS, USA. 4Fermi National Accelerator Laboratory, Batavia, IL, USA. 5 Joint Institute for Nuclear Research, Dubna, Russia. ⁶Universidad del Magdalena, Santa Marta, Colombia. ⁷Department of Physics and Astronomy, University of Sussex, Brighton, UK. ⁸Department of Physics, University of Cincinnati, Cincinnati, OH, USA. 9Instituto de Física, Universidade Federal de Goiás, Goiânia, Brazil. 10Indiana University, Bloomington, IN, USA. ¹¹Department of Physics and Astronomy, Iowa State University, Ames, IA, USA. 12 Department of Physics and Astronomy, University of California at Irvine, Irvine, CA, USA. ¹³School of Physics, University of Hyderabad, Hyderabad, India. ¹⁴Faculty of Engineering and Natural Sciences, Engineering Sciences Department, Bandırma Onyedi Eylül University, Bandırma, Turkey. 15 School of Physics and Astronomy, University of Minnesota Twin Cities, Minneapolis, MN, USA. ¹⁶Department of Physics, Panjab University, Chandigarh, India. 17 Department of Physics, IIT Guwahati, Guwahati, India. 18 Particle Physics Research Centre, Department of Physics and Astronomy, Queen Mary University of London, London, UK. ¹⁹Department of Physics, IIT Hyderabad, Hyderabad, India. ²⁰Department of Physics and Astronomy, Michigan State University, East Lansing, MI, USA. ²¹Department of Physics, Colorado State University, Fort Collins, CO, USA. ²²Institute for Nuclear Research of the Russian Academy of Sciences, Moscow, Russia. 23 Physics and Astronomy Department, University College London, London, UK. ²⁴Department of Physics, University of Texas at Austin, Austin, TX, USA. 25 Department of Physics, University of Wisconsin-Madison, Madison, WI, USA. ²⁶Department of Physics, William & Mary, Williamsburg, VA, USA. ²⁷Illinois Institute of Technology, Chicago, IL, USA. 28 Department of Physics and Astrophysics, University of Delhi, Delhi, India. ²⁹Department of Physics, Southern Methodist University, Dallas, TX, USA. ³⁰Department of Physics, University of Virginia, Charlottesville, VA, USA. ³¹Argonne National Laboratory, Argonne, IL, USA. 32 Department of Physics, University of Houston, Houston, TX, USA. 33 Department of Mathematics, Statistics and Physics, Wichita State University, Wichita, KS, USA. 34 Institute of Physics, The Czech Academy of Sciences, Prague, Czech Republic. 35Department of Physics, University of South Alabama, Mobile, AL, USA. 36Department of Physics and Astronomy, Tufts University, Medford, MA, USA. 37Department of Physics and Astronomy, University of Minnesota Duluth, Duluth, MN, USA. 38 Institute of Computer Science, The Czech Academy of Sciences, Prague, Czech Republic. 39 Department of Physics, Syracuse University, Syracuse, NY, USA. 40 Department of Physics and Astronomy, University of South Carolina, Columbia, SC, USA. 41 Czech Technical University in Prague, Prague, Czech Republic. ⁴²Department of Physics, Cochin University of Science and Technology, Kochi, India. ⁴³California Institute of Technology, Pasadena, CA, USA. ⁴⁴Department of Physics, University of Pittsburgh, Pittsburgh, PA, USA. 45 National Institute of Science Education and Research, Khurda, India. 46Florida State University, Tallahassee, FL, USA. 47Department of Physics, Institute of Science, Banaras Hindu University, Varanasi, India. ⁴⁸Faculty of Mathematics and Physics, Institute of Particle and Nuclear Physics, Charles University, Prague, Czech Republic. ⁴⁹Ohio State University, Columbus, OH, USA.

The T2K Collaboration

K. Abe⁵⁰, S. Abe⁵⁰, H. Adhkary⁵¹, R. Akutsu⁵², H. Alarakia-Charles⁵³, Y. I. Ali Hakim⁵⁴, S. Alonso Monsalve⁵⁵, L. Anthony⁵⁶, S. Aoki⁵⁷, K. A. Apte⁵⁶, T. Arai⁵⁸, T. Arihara⁵⁹, S. Arimoto⁶⁰, Y. Ashida⁶¹, E. T. Atkin⁵⁶, N. Babu⁶², V. Baranov⁵, G. J. Barker⁶³, G. Barr⁶⁴, D. Barrow⁶⁴, P. Bates⁶⁵, L. Bathe-Peters⁶⁴, M. Batkiewicz-Kwasniak⁶⁶, N. Baudis⁶⁴, V. Berardi⁶⁷, L. Berns⁶¹, S. Bhattacharjee⁶², A. Blanchet⁶⁸, A. Blondel^{69,70}, P. M. M. Boistier⁷¹, S. Bolognesi⁷¹, S. Bordoni⁶⁹, S. B. Boyd⁶³, C. Bronner⁷², A. Bubak⁷³, M. Buizza Avanzini⁷⁴, J. A. Caballero⁷⁵, F. Cadoux⁶⁹, N. F. Calabria⁶⁷, S. Cao⁷⁶, S. Cap⁶⁹, D. Carabadjac^{74,77}, S. L. Cartwright⁵⁴, M. P. Casado^{78,79}, M. G. Catanesi⁶⁷, J. Chakrani⁸⁰, A. Chalumeau⁷⁰, D. Cherdack³² A. Chvirova²², J. Coleman⁶⁵, G. Collazuol⁸¹, F. Cormier⁸², A. A. L. Craplet⁵⁶, A. Cudd⁸³, D. D'ago⁸¹, C. Dalmazzone⁷⁰, T. Daret⁷¹, P. Dasgupta⁸⁴, C. Davis⁸⁵, Yu. I. Davydov⁵, P. de Perio⁸⁶, G. De Rosa⁸⁷, T. Dealtry⁵³, C. Densham⁸⁸, A. Dergacheva²², R. Dharmapal Banerjee⁸ F. Di Lodovico⁹⁰, G. Diaz Lopez⁷⁰, S. Dolan⁶⁸, D. Douqa⁶⁹, T. A. Doyle⁹¹, O. Drapier⁷⁴, K. E. Duffy⁶⁴, J. Dumarchez⁷⁰, P. Dunne⁵⁶, K. Dygnarowicz⁹², A. Eguchi⁵⁸, J. Elias⁹³ S. Emery-Schrenk⁷¹, G. Erofeev²², A. Ershova⁷⁴, G. Eurin⁷¹, D. Fedorova²², S. Fedotov²² M. Feltre⁸¹, L. Feng⁶⁰, D. Ferlewicz⁵⁸, A. J. Finch⁵³, M. D. Fitton⁸⁸, C. Forza⁸¹, M. Friend^{52,94}, Y. Fujii⁵², Y. Fukuda⁹⁵, Y. Furui⁵⁹, J. García-Marcos⁹⁶, A. C. Germer⁸⁵, L. Giannessi⁶⁹,

C. Giganti⁷⁰, M. Girgus⁵¹, V. Glagolev⁵, M. Gonin⁹⁷, R. González Jiménez⁷⁵, J. González Rosa⁷⁵, E. A. G. Goodman⁹⁸, K. Gorshanov²², P. Govindaraj⁵¹, M. Grassi⁸¹, M. Guigue⁷⁰, F. Y. Guo⁹¹, D. R. Hadley⁶³, S. Han^{60,99}, D. A. Harris¹⁰⁰, R. J. Harris^{53,88}, T. Hasegawa^{52,94}, C. M. Hasnip⁶⁸ S. Hassani⁷¹, N. C. Hastings⁵², Y. Hayato^{50,86}, I. Heitkamp⁶¹, D. Henaff⁷¹, Y. Hino⁵², J. Holeczek⁷³, A. Holin⁸⁸, T. Holvey⁶⁴, N. T. Hong Van¹⁰¹, T. Honjo¹⁰², M. C. F. Hooft⁸⁶, K. Hosokawa⁵⁰, J. Hu⁶⁰, A. K. Ichikawa⁶¹, K. Ieki⁵⁰, M. Ikeda⁵⁰, T. Ishida^{52,94}, M. Ishitsuka¹⁰³, A. Izmaylov²², N. Jachowicz⁹⁶, S. J. Jenkins⁶⁵, C. Jesús-Valls⁸⁶, M. Jia⁹¹, J. J. Jiang⁹¹, J. Y. Ji⁹¹, T. P. Jones⁵³, P. Jonsson⁵⁶, S. Joshi⁷¹, C. K. Jung⁹¹, M. Kabirnezhad⁵⁶, A. C. Kaboth¹⁰⁴, H. Kakuno⁵⁹ J. Kameda⁵⁰, S. Karpova⁶⁹, V. S. Kasturi⁶⁹, Y. Kataoka⁵⁰, T. Katori⁹⁰, Y. Kawamura¹⁰², M. Kawaue⁶⁰, E. Kearns^{86,105}, M. Khabibullin²², A. Khotjantsev²², T. Kikawa⁶⁰, S. King⁹⁰, V. Kiseeva⁵, J. Kisiel⁷³, A. Klustová⁵⁶, L. Kneale⁵⁴, H. Kobayashi⁵⁸, L. Koch¹⁰⁶, S. Kodama⁵⁸, M. Kolupanova²², A. Konaka⁸², L. L. Kormos⁵³, Y. Koshio^{86,107}, K. Kowalik¹⁰⁸, Y. Kudenko²² Y. Kudo⁷², A. Kumar Jha⁹⁶, R. Kurjata⁹², V. Kurochka²², T. Kutter⁶², L. Labarga¹ K. Lachner⁵⁵, J. Lagoda¹⁰⁸, S. M. Lakshmi⁷³, M. Lamers James⁶³, A. Langella⁸ D. H. Langridge¹⁰⁴, J.-F. Laporte⁷¹, D. Last⁹³, N. Latham⁹⁰, M. Laveder⁸¹, L. Lavitola⁸⁷ M. Lawe⁵³, D. Leon Silverio¹¹⁰, S. Levorato⁸¹, S. V. Lewis⁹⁰, B. Li⁵⁵, C. Lin⁵⁶, R. P. Litchfield⁹⁸, S. L. Liu⁹¹, W. Li⁶⁴, A. Longhin⁸¹, A. Lopez Moreno⁹⁰, L. Ludovici¹¹¹, X. Lu⁶³, T. Lux⁷⁸, L. N. Machado⁹⁸, L. Magaletti⁶⁷, K. Mahn²⁰, K. K. Mahtani⁹¹, M. Mandal¹⁰⁸, S. Manlv⁹³ A. D. Marino⁸³, D. G. R. Martin⁵⁶, D. A. Martinez Caicedo¹¹⁰, L. Martinez⁷⁸, M. Martini^{70,112}, T. Matsubara⁵², R. Matsumoto¹¹³, V. Matveev²², C. Mauger⁸⁵, K. Mavrokoridis⁶⁵ N. McCauley⁶⁵, K. S. McFarland⁹³, C. McGrew⁹¹, J. McKean⁵⁶, A. Mefodiev²², G. D. Megias⁷⁵, L. Mellet²², C. Metelko⁶⁵, M. Mezzetto⁸¹, S. Miki⁵⁰, V. Miklola⁹⁶, E. W. Miller⁷⁸, A. Minamino⁷², O. Mineso²², S. Mine^{50,114}, J. Mirabito¹⁰⁵, M. Miura^{50,86}, S. Moriyama^{50,86}, S. Moriyama⁷², P. Morrison⁹⁸, Th. A. Mueller⁷⁴, D. Munford³², A. Muñoz^{74,97}, L. Munteanu⁶⁸, Y. Nagai⁸⁴ T. Nakadaira^{52,94}, K. Nakagiri⁵⁸, M. Nakahata^{50,96}, Y. Nakajima⁵⁸, K. D. Nakamura⁵¹, Y. Nakano¹¹⁵, S. Nakayama^{50,86}, T. Nakaya^{60,86}, K. Nakayoshi^{52,94}, C. E. R. Naseby⁵⁵, D. T. Nguyen¹¹⁶, V. Q. Nguyen⁷⁴, K. Niewczas⁹⁶, S. Nishimori⁵², Y. Nishimura¹¹⁷, Y. Noguchi⁵⁰, T. Nosek¹⁰⁸, F. Nova⁸⁸, J. C. Nugent⁵⁶, H. M. O'Keeffe⁵³, L. O'Sullivan¹⁰⁶, R. Okazaki¹¹⁷, W. Okinaga⁵⁸, K. Okumura^{86,99}, T. Okusawa¹⁰², N. Onda⁶⁰, N. Ospina⁶⁷, L. Osu⁷⁴, Y. Oyama^{52,94}, V. Paolone¹¹⁸, J. Pasternak⁵⁶, D. Payne⁶⁵, T. Peacock⁵⁴, M. Pfaff⁵⁶, L. Pickering⁸⁸, B. Popov^{5,70} A. J. Portocarrero Yrey⁵², M. Posiadala-Zezula⁵¹, Y. S. Prabhu⁵¹, H. Prasad⁸⁹, F. Pupilli⁸¹ B. Quilain^{74,97}, P. T. Quyen^{76,119}, E. Radicioni⁶⁷, B. Radics¹⁰⁰, M. A. Ramirez⁸⁵, R. Ramsden⁹⁰ P. N. Ratoff⁵³, M. Reh⁸³, G. Reina¹⁰⁶, C. Riccio⁹¹, D. W. Riley⁹⁸, E. Rondio¹⁰⁸, S. Roth¹²⁰, N. Roy¹⁰⁰, A. Rubbia⁵⁵, L. Russo⁷⁰, A. Rychter⁹², W. Saenz⁷⁰, K. Sakashita^{52,94}, S. Samani⁶⁹, F. Sánchez⁶⁹, E. M. Sandford⁶⁵, Y. Sato¹⁰³, T. Schefke⁶², C. M. Schloesser⁶⁹, K. Scholberg^{86,121}, M. Scott⁵⁶, Y. Seiya^{102,122}, T. Sekiguchi^{52,94}, H. Sekiya^{50,86}, T. Sekiya⁵⁹, D. Seppala²⁰, D. Sgalaberna⁵⁵, A. Shaikhiev²², M. Shiozawa^{50,86}, Y. Shiraishi¹⁰⁷, A. Shvartsman²², N. Skrobova²¹ K. Skwarczynski¹⁰⁴, D. Smyczek¹²⁰, M. Smy¹¹⁴, J. T. Sobczyk⁸⁹, H. Sobel^{86,114}, F. J. P. Soler⁹⁸ A. J. Speers⁵³, R. Spina⁶⁷, A. Srivastava¹⁰⁶, P. Stowell⁵⁴, Y. Stroke²², I. A. Suslov⁵, A. Suzuki⁵⁷, S. Y. Suzuki^{52,94}, M. Tada^{52,94}, S. Tairafune⁶¹, A. Takeda⁵⁰, A. Teklu⁹¹, Y. Takeuchi^{57,86} H. K. Tanaka^{50,86}, H. Tanigawa⁵², V. V. Tereshchenko⁵, N. Thamm¹²⁰, C. Touramanis⁶⁵, N. Tran⁶⁰, T. Tsukamoto^{52,94}, M. Tzanov⁶², Y. Uchida⁵⁶, M. Vagins^{86,114}, M. Varghese⁷ I. Vasilyev⁵, G. Vasseur⁷¹, E. Villa^{68,69}, U. Virginet⁷⁰, T. Vladisavljevic⁸⁸, T. Wachala⁶⁶ D. Wakabayashi⁶¹, H. T. Wallace⁵⁴, J. G. Walsh²⁰, L. Wan¹⁰⁵, D. Wark^{64,88}, M. O. Wascko^{64,88} A. Weber¹⁰⁶, R. Wendell⁶⁰, M. J. Wilking¹²³, C. Wilkinson⁸⁰, J. R. Wilson⁹⁰, K. Wood⁸⁰, C. Wret⁵⁶, J. Xia¹²⁴, K. Yamamoto^{102,122}, T. Yamamoto¹⁰², C. Yanagisawa^{91,125}, Y. Yang⁶⁴, T. Yano⁵⁰, N. Yershov²², U. Yevarouskaya⁹¹, M. Yokoyama^{58,86}, Y. Yoshimoto⁵⁸, N. Yoshimura⁶⁰, R. Zaki¹⁰⁰, A. Zalewska⁶⁶, J. Zalipska¹⁰⁸, G. Zarnecki⁶⁶, J. Zhang^{82,126}, X. Y. Zhao⁵⁵, H. Zheng⁹¹, H. Zhong⁵⁷, T. Zhu⁵⁶, M. Ziembicki⁹², E. D. Zimmerman⁸³, M. Zito⁷⁰ & S. Zsoldos⁹⁰

⁵⁰University of Tokyo, Institute for Cosmic Ray Research, Kamioka Observatory, Kamioka, Japan. ⁵¹Faculty of Physics, University of Warsaw, Warsaw, Poland. ⁵²High Energy Accelerator Research Organization (KEK), Tsukuba, Japan. 53 Physics Department, Lancaster University, Lancaster, United Kingdom. 54 School of Mathematical and Physical Sciences, University of Sheffield, Sheffield, United Kingdom. 55 Institute for Particle Physics and Astrophysics, ETH Zurich, Zurich, Switzerland. 56 Department of Physics, Imperial College London, London, United Kingdom. ⁷⁷Kobe University, Kobe, Japan. ⁵⁸Department of Physics, University of Tokyo, Tokyo, Japan. ⁵⁹Department of Physics, Tokyo Metropolitan University, Tokyo, Japan. ⁶⁰Department of Physics, Kyoto University, Kyoto, Japan. ⁶¹Faculty of Science, Department of Physics, Tohoku University, Miyagi, Japan, 62 Department of Physics and Astronomy, Louisiana State University, Baton Rouge, LA, USA. ⁶³Department of Physics, University of Warwick, Coventry, UK. ⁶⁴Department of Physics, Oxford University, Oxford, UK. ⁶⁵Department of Physics, University of Liverpool, Liverpool, UK. 66The Henryk Niewodniczanski Institute of Nuclear Physics, Polish Academy of Sciences, Cracow, Poland. ⁶⁷Dipartimento Interuniversitario di Fisica, Università e Politecnico di Bari and INFN Sezione di Bari, Bari, Italy, ⁶⁸European Organization for Nuclear Research (CERN), Geneva, Switzerland. ⁶⁹DPNC, Section de Physique, University of Geneva, Geneva, Switzerland. Laboratoire de Physique Nucléaire et de Hautes Energies (LPNHE), Sorbonne Université, CNRS/IN2P3, Paris, France. 71 IRFU, CEA, Université Paris-Saclay, Gif-sur-Yvette, France. ⁷²Department of Physics, Yokohama National University, Yokohama, Japan. ⁷³Institute of Physics, University of Silesia, Katowice, Poland. 74 Laboratoire Leprince-Ringuet, Ecole Polytechnique, IN2P3-CNRS, Palaiseau, France. 75 Departamento de Física Atómica, Molecular y Nuclear, Universidad de Sevilla, Sevilla, Spain. 76 Institute for Interdisciplinary Research in Science and Education (IFIRSE), International Centre for Interdisciplinary Science and Education, Quy Nhon, Vietnam. 77 Université Paris-Saclay, Gif-sur-Yvette, France. 78 Institut de Fisica d'Altes Energies (IFAE), The Barcelona Institute of Science and Technology, Universitat Autònoma de Barcelona, Barcelona, Spain. ⁷⁹Departament de Fisica, Universitat Autònoma de Barcelona, Barcelona, Spain. ⁸⁰Lawrence Berkeley National Laboratory, Berkeley, CA, USA ⁸¹Dipartimento di Fisica, INFN Sezione di Padova, Università di Padova, Padova, Italy. ⁸²TRIUMF, Vancouver, BC, Canada. 83 Department of Physics, University of Colorado Boulder, Boulder, CO, USA. 84 Department of Atomic Physics, Eötvös Loránd University, Budapest, Hungary. ⁸⁵Department of Physics and Astronomy, University of Pennsylvania, Philadelphia, PA, USA. 86 Kavli Institute for the Physics and Mathematics of the Universe (WPI), The University of Tokyo Institutes for Advanced Study, University of Tokyo, Kashiwa, Japan. ⁸⁷Dipartimento di Fisica, INFN Sezione di Napoli, Università di Napoli, Napoli, Italy. 88STFC, Rutherford Appleton Laboratory, Didcot, UK. 89 Faculty of Physics and Astronomy, Wroclaw University, Wroclaw, Poland. 90 Department of Physics, King's College London, London, UK. 91 Department of Physics and Astronomy, State University of New York at Stony Brook, Stony Brook, NY, USA, 92 Institute

of Radioelectronics and Multimedia Technology, Warsaw University of Technology, Warsaw, Poland. 93Department of Physics and Astronomy, University of Rochester, Rochester, NY, USA. 94 Japan Proton Accelerator Research Complex, Tokai, Japan. 95 Department of Physics, Miyagi University of Education, Sendai, Japan. 96 Department of Physics and Astronomy, Ghent University, Gent, Belgium. 97ILANCE, CNRS, University of Tokyo International Research Laboratory, Kashiwa, Japan. 98 School of Physics and Astronomy, University of Glasgow, Glasgow, UK. 99 Research Center for Cosmic Neutrinos, Institute for Cosmic Ray Research, University of Tokyo, Kashiwa, Japan. 100 Department of Physics and Astronomy, York University, Toronto, Ontario, Canada. 101 International Centre of Physics, Institute of Physics (IOP), Vietnam Academy of Science and Technology (VAST), Hanoi, Vietnam. 102 Department of Physics, Osaka Metropolitan University, Osaka, Japan. 103 Department of Physics, Tokyo University of Science, Faculty of Science and Technology, Noda, Chiba, Japan. 104 Department of Physics, Royal Holloway University of London, Egham, UK. 105 Department of Physics, Boston University, Boston, MA, USA. ¹⁰⁶Institut für Physik, Johannes Gutenberg-Universität Mainz, Mainz, Germany. ⁰⁷Department of Physics, Okayama University, Okayama, Japan. ¹⁰⁸National Centre for Nuclear Research, Warsaw, Poland. 109 Department of Theoretical Physics, University Autonoma Madrid,

Madrid, Spain. 110 South Dakota School of Mines and Technology, Rapid City, SD, USA. 111 INFN Sezione di Roma and Università di Roma "La Sapienza", Roma, Italy. 112 IPSA-DRII, Ivry-sur-Seine, France. 113 Department of Physics, Institute of Science Tokyo, Tokyo, Japan. 114 Department of Physics and Astronomy, University of California, Irvine, Irvine, CA, USA. ¹¹⁵Department of Physics, University of Toyama, Toyama, Japan. 116 VNU University of Science, Vietnam National University, Hanoi, Vietnam. ¹¹⁷Department of Physics, Keio University, Kanagawa, Japan. ¹¹⁸Department of Physics and Astronomy, University of Pittsburgh, Pittsburgh, PA, USA. ¹¹⁹Graduate University of Science and Technology, Vietnam Academy of Science and Technology, Hanoi, Vietnam. 120 III. Physikalisches Institut, RWTH Aachen University, Aachen, Germany. 121 Department of Physics, Duke University, Durham, NC, USA. 122 Nambu Yoichiro Institute of Theoretical and Experimental Physics, Osaka, Japan. 123 School of Physics and Astronomy, University of Minnesota, Minneapolis, MN, USA. 124 SLAC National Accelerator Laboratory, Stanford University, Menlo Park, CA, USA. 125 Science Department, Borough of Manhattan Community College, City University of New York, New York, NY, USA. 126 Department of Physics and Astronomy, University of British Columbia, Vancouver, British Columbia, Canada.

Methods

The NOvA experiment

The NOvA experiment measures neutrino oscillations using two detectors of functionally identical construction located along the NuMI neutrino beam⁵⁰ produced at the Fermi National Accelerator Laboratory (Fermilab).

The smaller 0.3-kt near detector is located on the Fermilab campus 1 km downstream from the neutrino production target, whereas the 14-kt far detector is located 810 km away in northern Minnesota. The detectors themselves are highly segmented tracking calorimeters consisting of long PVC cells filled with a mineral-oil-based liquid scintillator. Each cell measures 6.6 cm × 3.9 cm in cross-section, runs the full height or width of the detector (15.5 m for the far detector and 3.9 m for the near detector) and is instrumented with a wavelength-shifting fibre and avalanche photodiode to detect the scintillation light produced when charged particles pass through the cell. The cells are arranged in a series of layers, each with either horizontal or vertical orientation, with the direction alternating between layers to provide three-dimensional (3D) event reconstruction. This segmented design offers the excellent muon and electron classification needed for tagging the incoming neutrino flavour. In particular, electromagnetic showers at typical NOvA energies are much larger than the detector cell widths and thus are well-imaged and distinct from many potential backgrounds. The detectors of NOvA are centred 14.6 mrad off the central axis of the NuMI beam, yielding a narrow-band neutrino beam peaked at 1.8 GeV.

As is typical for particle physics experiments, NOvA makes use of detailed simulations of beam production, neutrino interaction physics and detector response as part of the analysis. Given the matching near and far detectors, NOvA forms its oscillation-dependent predictions of the far-detector event rates directly from data using the millions of neutrino interactions recorded in the near detector. This near-to-far extrapolation process is carried out as a function of multiple kinematic and event classification variables. Uncertainties from the simulations have substantially reduced impact as they enter the oscillation fit only to the extent that they affect the mapping between expected near and far event rates, not the event rates of the individual detectors themselves. Uncertainties on the simulations are taken as the a priori uncertainties from, for instance, the external model constraints or other external data and are supplemented by additional model uncertainties in which a priori coverage was deemed unsatisfactory.

Far-detector data are fitted to the corresponding far-detector predictions to extract oscillation parameter constraints. These data are separated by beam mode (that is, neutrino- or antineutrino-dominated running) and further into v_μ/\bar{v}_μ charged current and v_e/\bar{v}_e charged current candidate samples using a convolutional neural network those inputs are the calibrated event images recorded by the detector cells. Subsequent reconstruction of tracks and showers within each event provides kinematic information such as estimated neutrino energy. Far detector v_μ/\bar{v}_μ samples are analysed in bins of neutrino energy and hadronic energy fraction. The v_e/\bar{v}_e samples are analysed in bins related to event containment, event classification score and neutrino energy. More details on the analysis techniques, simulation packages, systematic uncertainties and the overall NOvA experimental design can be found in ref. 13 and the references therein.

The T2K experiment

The T2K experiment is composed of the J-PARC neutrino beam, a near site with multiple detectors and the water Cherenkov detector Super-Kamiokande (SK) as the far detector. Full details of the experiment can be found in ref. 25.

The primary detector at the near site, 280 m from the target, is a magnetized off-axis (centred at 43.6 mrad) tracking detector called ND280. While taking the data used in this analysis, ND280 consisted

of a π^0 detector followed by a tracker consisting of three time-projection chambers interleaved with two hydrocarbon fine-grained detectors (FGD1 and FGD2), all surrounded by an electromagnetic calorimeter. The stability and direction of the neutrino beam are monitored using the on-axis near detector INGRID.

SK is situated 295 km downstream of the neutrino production target, 43.6 mrad off-axis, and contains 50 kt of water. An inner detector (ID) using 11,129 inward-facing 20-inch photomultiplier tubes (PMTs) detects Cherenkov radiation from charged particles traversing the detector. An optically separated outer detector uses 1,885 outward-facing 8-inch PMTs to reject interactions originating outside the ID volume. SK can discriminate between electrons and muons by their Cherenkov ring profiles.

T2K uses a forward-fitting analysis strategy. First, a model that predicts the event spectra at the near and far detectors is defined and tuned to external experimental data. The predictions are generated by simulating the neutrino flux and cross-section as well as the detector response. The model, with variable parameters, is fit to the ND280 data to obtain tuned values of the parameters with uncertainties. The constrained model resulting from this near-detector fit is then used to make SK predictions, which are fit to the SK data to extract oscillation parameters. Complete details for this analysis, including model details, are in ref. 14.

T2K splits data at the near and far detectors into mutually exclusive samples defined by particle identification in each beam mode. At ND280, events are categorized into 18 samples, nine samples in each of FGD1 and FGD2. In neutrino mode, data with one negatively charged muon is split into three samples in each FGD corresponding to the number of pions (0, 1, or >1). In antineutrino mode, data are first split by whether a negatively or positively charged muon is present, and then divided by the number of pions as in the neutrino-mode data, forming six samples in each FGD. For all samples, the data are fit in a 2D space of the muon momentum and the angle between the muon and the average beam direction. The exclusive samples allow the near-detector fit to better constrain parameters related to different neutrino-nucleus interaction modes. At SK, the data are divided into three samples in neutrino mode: one-ring muon-like, one-ring electron-like and one-ring electron-like with one decay electron; in antineutrino mode, only the one-ring muon-like and one-ring electron-like samples are used. The data are binned in reconstructed neutrino energy. All electron-like samples are additionally binned in a second dimension, the angle between the reconstructed electron direction and the beam direction.

Detector systematic uncertainties are evaluated using a variety of sideband samples and calibrations, covering effects such as particle identification, particle momentum reconstruction, secondary particle interactions and fiducial volume effects.

Correlations in flux modelling

The modelling of the neutrino flux depends on many details relating to the incident proton beam, the hadron production target and the magnetic focusing horns. As these details are specific to each experiment, flux systematic uncertainties due to magnetic field variations, component alignment and other beamline properties are uncorrelated between the experiments.

The only possible correlation identified was the pion and kaon production models and the use of hadron interaction experiments to tune them 52,53 . In the case of NOvA, the primary data are from the NA49 experiment 33 , which collected thin-target (slices of the target material) data at 158 GeV c^{-1} , which is then scaled to the NuMI beam energy. The NA61/SHINE experiment, which collected data for T2K, uses some of the same detectors and the same beamline as NA49. NA61/SHINE 34,35 collected both thin-target and replica-target (a full-sized target) data for T2K at 31 GeV c^{-1} , the J-PARC beam momentum. Checking the consistency of the NA49 and NA61/SHINE data used is difficult, as the data are collected at different beam energies.

The NOvA experiment primarily uses thin-target NA49 hadron production data to tune the particle multiplicities, reweighting interactions and particle propagation inside the target and other beamline materials. By contrast, T2K uses thin and replica-target data from NA61/SHINE to reweight the multiplicities of particles exiting the target. Given these differences in data collection and tuning methodology, and given that flux uncertainties have a suppressed influence after ND data constraints are considered, there is no expectation of significant correlations between flux systematic parameters for NOvA and T2K in the joint fit.

Correlations in detector modelling

The experiments use different detector technologies as well as strategies for forming data samples, which removes most opportunities for correlation. However, the modelling of particle propagation through the detectors derives from the same underlying physics. This propagation is called secondary interaction (SI), and the case of pion SI is noteworthy, as this process is expected to occur in both experiments, and for T2K, it is an important effect. T2K selects exclusive data samples in which a change in reconstructed pion multiplicity can cause migration between samples. By contrast, NOvA uses inclusive selections, and pion SI has minimal effect on the calorimetric energy estimation at NOvA. Thus, we do not expect significant correlations due to pion SI.

Tests of individual parameter correlations

Neutrino-on-nucleus scattering plays a central part in both experiments, but the modelling of this physics has substantial differences between the two individual analyses. These differences, together with the presence of different nuclear targets, neutrino energies and near-detector strategies, mean that direct estimation of systematic uncertainty correlations in the neutrino scattering models is highly non-trivial. As part of this analysis, we tested how significant inter-experimental systematic uncertainty correlations could be, starting by identifying the most impactful systematic uncertainties of T2K and NOvA and exploring correlations between them.

To determine an impactful systematic parameter, we carry out a fit to pseudo-data generated with all parameters at their prior values from our nominal model. Then, for each parameter in turn, we reweight all steps from the obtained MCMC chain to have a tight ('shrunk') prior for that parameter around a different value ('pulled') to that used to generate the pseudo-data and study the change in the extracted oscillation parameter intervals. This procedure mocks up the result of an external experiment, providing a strong constraint on each systematic parameter at a different value from that preferred by simulated pseudo-data. This 'shrink and pull' study allows for assessing the single-parameter impact on the systematic uncertainty and the estimated credible intervals of the measurement of the individual neutrino oscillation parameters.

First, we identify both the systematic parameters of NOvA and T2K with the largest impact on $\delta_{\rm CP}$, $\sin^2\theta_{23}$ and Δm_{32}^2 in the joint fit.

For both experiments, the largest change in $\delta_{\rm CP}$ credible interval comes from uncertainties on $\nu_{\rm e}$ and $\overline{\nu}_{\rm e}$ normalizations. As discussed, these uncertainties are implemented identically in both experiments, and we have correlated them in the joint analysis. No additional interaction uncertainties in our models have any significant impact on the resulting credible intervals of $\delta_{\rm CP}$.

For $\sin^2\theta_{23}$, all the individual interaction systematic parameters have very small effects, changing the width of the 1σ interval by less than 2% when shrunk by 50% and pulled 1σ away from the nominal value. The largest change in credible interval comes from the uncertainty on the neutron visible energy for NOvA, and the two-particle two-hole (2p2h) C/O cross-section scale for T2K (2p2h C/O cross-section scale allows the 2p2h cross-section on carbon to differ from that for oxygen). For Δm_{32}^2 , all the individual interaction parameters have a negligible effect on the resulting Δm_{32}^2 credible intervals. Hence, we widened the list of

considered parameters and identified the calorimetric energy scale uncertainty of NOvA and the SK energy scale uncertainty of T2K as the most impactful for Δm_{32}^2 .

Second, despite there being no a priori reason to expect correlations between these specific parameters, we test whether or not correlating the most impactful T2K parameter with the most impactful NOvA parameter modifies oscillation parameter constraints in the joint fit in a significant way. We simulate pseudo-data to which we perform a joint fit while treating the T2K and NOvA parameters described above as either uncorrelated, fully correlated or fully anticorrelated. We repeat the study for each pair of the most impactful parameters of T2K and NOvA with respect to δ_{CP} , $\sin^2\theta_{23}$ and Δm_{32}^2 . In the case of Δm_{32}^2 , we further inflate the original SK energy scale uncertainty from 2% to 7% to amplify the effect. Finally, we check the extracted 1σ and 2σ credible regions for any substantial differences between the three correlation configurations. These tests are repeated for three sets of pseudo-data generated with oscillation parameter values that are T2K-like, NOvA-like and NuFit-like⁵⁴, which are chosen to be close to recent data results from the respective collaborations and are given in Extended Data Table 1.

As an example, Extended Data Fig. 1 shows the results in terms of the posterior probability distributions and credible regions of the parameters of interest from the set of fits with the largest single-parameter impact on $\sin^2\theta_{23}$. We conclude that the choice of correlation between single parameters does not significantly change the oscillation parameter constraints derived from the current version of the joint analysis.

Nightmare parameters

As described in the main text, we study correlations in more extreme situations using the so-called nightmare parameters, which are either artificially constructed parameters or existing parameters with highly inflated uncertainties chosen to be deliberately problematic for the individual analyses. The prior uncertainties of the parameters are set so that they are comparable in impact to the statistical uncertainties on the measurements under study. We carry out this procedure separately for simulated measurements of Δm_{32}^2 and θ_{23} . No nightmare study was carried out for $\delta_{\rm CP}$ because its total systematic uncertainty compared with the statistical uncertainty is much smaller than for the other two cases.

We construct pseudo-datasets with both the NOvA and T2K nightmare parameters shifted by one standard deviation from their prior values, inducing a systematic bias representing a simultaneous and coordinated shift in both NOvA and T2K data. We fit this pseudo-data while treating the NOvA and T2K nightmare parameters as either fully $correlated, uncorrelated\ or\ anticorrelated.\ The\ results\ of\ the\ night mare$ parameters correlation study are presented as 1 \u03c4 credible 2D regions of $\Delta m_{32}^2 - \sin^2 \theta_{23}$ in Extended Data Fig. 2 for both nightmare scenarios. We conclude that there is no significant difference in treating the nightmare parameters as either fully correlated (matching the pseudo-data) or uncorrelated between the experiments, whereas the incorrect anticorrelated case yields a clear bias. We note that these are not general conclusions but are specific to the T2K and NOvA analysis versions and cumulative beam exposures used here. The construction of the nightmare parameters is also not a unique choice, and other formulations of the parameters could be considered.

Out-of-model variations

As described in the main text, we use a set of discrete changes to the base cross-section model to test the robustness of our analysis. For each test, pseudo-data are generated assuming the specific model variation, and these pseudo-data are then fit either with the default analysis directly, which does not incorporate the model variation ('out-of-model' case) or with a modified analysis that has had its nominal event spectra altered to match the spectra expected under the varied model ('in-model' case). Between these two cases, we require that the width of each of the extracted oscillation parameter intervals changes by no more than

10% (representing a small 'error on the error') and that the centre of the interval does not move by more than 50% of the systematic uncertainty (indicating adequate systematic uncertainty coverage of the tested out-of-model variation). Furthermore, we require that taking the largest changes seen across these studies does not affect the stated conclusions on CP violation or mass ordering determination for the analysis.

Three variations were chosen to perform the out-of-model studies:

- MINERvA 1 π : this model suppresses charged current (CC) and neutral current (NC) resonant pion production at low Q^2 to ensure good agreement between the MINERvA data⁵⁵ and the implementation of the Rein–Seghal model in the GENIE v.2 neutrino interaction simulation software³⁷.
- Non quasi-elastic (non-QE): in the T2K oscillation analysis¹⁴, the ND280 data samples with a muon candidate and zero pion candidates are underpredicted by the pre-fit T2K nominal model by 10% in both FGDs, which the fit accounts for by enhancing the charged current quasi-elastic (CCQE) interaction rate. To check this large freedom does not cause bias, an alternate model is produced, in which this underprediction is attributed to only non-QE processes.
- Pion SI: the pion SI model in the GEANT4 detector simulation toolkit
 was replaced with the Salcedo-Oset model⁵⁷ implemented in the NEUT generator³⁶, tuned to π-A scattering data⁵⁸.

We also used this process to study what happens when fitting pseudo-data constructed for both experiments using the nominal cross-section model of one or the other experiment (T2K-like and NOvA-like studies).

We show example results here for the MINERvA 1π case. Extended Data Fig. 3a,b shows the effect of this alternative model on event spectra used in the analysis. Note that not all event spectra are uniformly binned. Extended Data Figs. 3c-g and 4 compare the in-model and out-of-model fit results. No failures of our criteria are seen in any of the cases. More generally, no significant bias is seen in this joint fit for any of the model variations studied across any of the three tested sets of oscillation parameter values.

Some more recent T2K analyses 45 did see criteria failures when considering an alternative nuclear model, HF-CRPA 59 , and as a result widened their Δm_{32}^2 intervals. Both NOvA and T2K have independently studied the impact of the HF-CRPA model on the analyses used in this joint result, and we estimate that any potential effects in the context of this joint fit are within the thresholds set for our out-of-model variation tests.

Goodness of fit

The posterior-predictive *P*-value⁴¹ technique is used to determine whether a model provides a good fit to the data it is confronted with. We require that the posterior-predictive P-value to obtain the far-detector data in all samples, given the joint post-fit model, is greater than 0.05. We also check the P-values for individual far-detector samples and require that they are greater than 0.05 after allowing for the look-elsewhere effect, using the Bonferroni correction 60. All the P-values from the joint fit are shown in Extended Data Table 2. All the P-values (both total and split sample by sample) are within our acceptable range (>0.05), even without taking the look-elsewhere effect into account. This means that the model used in this joint fit—that is, the systematic models of the individual experiments with a shared oscillation parameter model—fits our data well, even when looking at individual samples. The P-values are consistent with previous T2K-only and NOvA-only analyses. The P-value considering rate and shape for all T2K samples in a T2K-only fit is 0.73, whereas the *P*-value considering all T2K samples in the joint fit is 0.75. Similarly, the P-values for all NOvA samples are 0.56 (NOvA-only fit) and 0.64 (joint fit).

Example posterior predictions 61 of the spectra for the ν_{μ} and ν_{e} subsamples of both experiments, overlaid over the observed data, are shown in Extended Data Fig. 5.

Priors

The default priors on the oscillation parameters for this analysis are as follows: flat between $-\pi$ and π in δ_{CP} , flat between 0 and 1 in $\sin^2\theta_{23}$, flat in Δm_{32}^2 and Gaussian with $\mu \pm \sigma = (2.18 \pm 0.07) \times 10^{-2}$ in $\sin^2\theta_{13}$. Where alternate priors are used, this is stated in the text.

This analysis is not sensitive to the oscillation parameters $\sin^2\theta_{12}$ and Δm_{21}^2 beyond existing experimental constraints; their Gaussian priors are set to be $\sin^2\theta_{12}=0.307\pm0.013$ and $\Delta m_{21}^2=(7.53\pm0.18)\times10^{-5}$ eV². These values, along with a Gaussian prior on $\sin^2\theta_{13}$, when it is used, come from the 2020 version of the Particle Data Group (PDG) summary tables⁴⁰, which were current at the time of the original analyses. Updates to these constraints in more recent versions of the PDG do not change any conclusions.

As well as the standard prior flat in δ_{CP} , we also studied the effect of a prior flat in $\sin \delta_{CP}$ and saw no significant changes in conclusions.

Moreover, the experiments define priors for all of the systematic parameters in their models. These definitions are detailed in the individual experiment analyses underlying this work.

Highest posterior probability values and 1σ credible intervals

Extended Data Table 3 summarizes the highest posterior probability values and credible intervals measured jointly by NOvA and T2K.

Additional oscillation parameter plots

The main text shows the 1D posterior distributions and credible intervals for the Jarlskog invariant, δ_{CP} and $\sin^2\theta_{23}$, as well as 2D distributions and credible regions for the latter two. In this section, we present the 1D distributions and credible intervals for δ_{CP} , $\sin^2\theta_{23}$, $\sin^22\theta_{13}$ and $|\Delta m_{32}^2|$, and 2D distributions and credible regions for all pairwise combinations of these parameters. These are shown in Extended Data Figs. 6–8, for the cases of marginalized over both mass orderings, conditional on the normal ordering and conditional on the inverted ordering, respectively. The distributions and intervals are shown in a triangle plot, in which a lower triangular matrix of plots shows the 1D distributions along the diagonal and the 2D distributions in each of the off-diagonal positions.

Reactor Δm_{32}^2

The energy-dependent $\overline{v}_{\rm e} \rightarrow \overline{v}_{\rm e}$ oscillation probability measured by reactor experiments is sensitive to $|\Delta m_{32}^2|$, and reactor measurements of this parameter are expected to agree with long-baseline measurements only under the correct mass ordering assumption. Under the incorrect ordering assumption, these two techniques are expected to measure incorrect values that differ from one another by about 2–3% (ref. 62). Thus, comparing $|\Delta m_{32}^2|$ measurements from accelerator and reactor experiments under both mass ordering hypotheses can inform mass ordering discrimination. The Daya Bay experiment⁴⁷ provides the tightest constraints on θ_{13} and also reports a 2D θ_{13} – Δm_{32}^2 likelihood that we can directly incorporate into our joint fit instead of the θ_{13} -only prior discussed elsewhere in this study.

The mass ordering Bayes factor obtained when using this 2D reactor constraint is 1.4 in favour of the normal ordering, in contrast to 1.3 in favour of the inverted ordering when using the $\theta_{\rm 13}$ -only reactor constraint. This slight pull towards a preference for the normal ordering is expected, given the relative agreement of the Daya Bay and NOvA+T2K $|\Delta m_{32}^2|$ measurements shown in Fig. 2 (inverted ordering) and Extended Data Fig. 9a (normal ordering). However, there remains no statistically significant mass ordering preference in this combination.

Additional global comparisons

In Extended Data Fig. 9, results of the analysis using the default priors are compared with other experimental measurements. The statement on Δm_{32}^2 precision is still valid for the normal ordering assumption. As in the case of the $\sin^2 2\theta_{13}$ result (Extended Data Fig. 9b,c), the

long-baseline measurements (in this comparison, without applying the prior from reactor measurements) are consistent with reactor experiments, with larger consistency in the normal ordering than the inverted ordering. We do not strongly prefer either octant of $\sin^2\!\theta_{23}$ (Extended Data Fig. 9d,e), which is consistent with other modern experiments. The joint analysis result for $\delta_{\rm CP}$ (Extended Data Fig. 9f,g) is consistent with all experiments and their combinations, although the uncertainty remains large.

Data availability

Inquiries regarding the data and posteriors used in this result may be directed to the collaborations.

Code availability

The NOvA and T2K collaborations develop and maintain the code used for the simulation of the experimental apparatus and statistical analysis of the raw data used in this result. This code is shared among the collaborations, but because of the size and complexity of the codebases, it is not publicly distributed. Inquiries regarding the algorithms and methods used in this result may be directed to the collaborations.

- Adamson, P. et al. The NuMI neutrino beam. Nucl. Instrum. Methods Phys. Res. A 806, 279–306 (2016).
- Aurisano, A. et al. A convolutional neural network neutrino event classifier. J. Instrum. 11, P09001 (2016).
- 52. Abe, K. et al. T2K neutrino flux prediction. Phys. Rev. D 87, 012001 (2013).
- Aliaga, L. et al. Neutrino flux predictions for the NuMI Beam. Phys. Rev. D 94, 092005 (2016).
- Esteban, I., Gonzalez-Garcia, M. C., Maltoni, M., Schwetz, T. & Zhou, A. The fate of hints: updated global analysis of three-flavor neutrino oscillations. J. High Energy Phys. 2020, 178 (2020).
- Stowell, P. et al. Tuning the GENIE pion production model with MINERvA data. Phys. Rev. D 100, 072005 (2019).
- Agostinelli, S. et al. GEANT4-a simulation toolkit. Nucl. Instrum. Methods Phys. Rev. A 506, 250–303 (2003).
- Salcedo, L. L., Oset, E., Vicente-Vacas, M. J. & Garcia-Recio, C. Computer simulation of inclusive pion nuclear reactions. *Nucl. Phys. A* 484, 557–592 (1988).
- Pinzon Guerra, E. S. et al. Using world π^e-nucleus scattering data to constrain an intranuclear cascade model. *Phys. Rev. D* 99, 052007 (2019).
- Pandey, V., Jachowicz, N., Van Cuyck, T., Ryckebusch, J. & Martini, M. Low-energy excitations and quasielastic contribution to electron-nucleus and neutrino-nucleus scattering in the continuum random-phase approximation. *Phys. Rev. C* 92, 024606 (2015).
- 60. Dunn, O. J. Multiple comparisons among means, J. Am. Stat. Assoc. 56, 52–64 (1961).
- 61. Gelman, A. et al. Bayesian Data Analysis 3rd edn (CRC Press, 2013).
- Parke, S. J. & Zukanovich-Funchal, R. Mass ordering sum rule for the neutrino disappearance channels in T2K, NOvA, and JUNO. Phys. Rev. D 111, 013008 (2025).
- 63. The Double Chooz Collaboration Double Chooz θ_{13} measurement via total neutron capture detection. *Nat. Phys.* **16**, 558–564 (2020).

Acknowledgements We thank the Fermi National Accelerator Laboratory (Fermilab), a US Department of Energy, Office of Science, HEP User Facility. Fermilab is managed by the Fermi Forward Discovery Group, acting under contract no. 89243024CSC000002. This work was supported by the US Department of Energy, including through the US-Japan Science and Technology Cooperation Program in HEP; the US National Science Foundation; the Department of Science and Technology, India; the European Research Council; the MSMT CR, GA UK, Czech Republic; the RAS, the Ministry of Science and Higher Education, and RFBR, Russia; CNPq and FAPEG, Brazil; UKRI, STFC and the Royal Society, UK; and the state and University of Minnesota. We are grateful for the contributions of the staff of the University of Minnesota at the Ash River Laboratory and of Fermilab. We thank the J-PARC staff for superb accelerator performance. We thank the CERN NA61/SHINE Collaboration for providing valuable particle production data. We acknowledge the support of MEXT, JSPS KAKENHI and bilateral programmes, Japan; NSERC, the NRC, and CFI, Canada; the CEA and CNRS/IN2P3 France; the Deutsche Forschungsgemeinschaft (DFG 397763730 and 517206441), Germany; the NKFIH (NKFIH 137812 and TKP2021-NKTA-64), Hungary; the INFN, Italy; the Ministry of Science and Higher Education (2023/WK/04) and the National Science Centre (UMO-2018/30/F/ST2/00441. UMO-2022/46/F/ST2/00336 and UMO-2021/43/D/ST2/01504). Poland: the RSF (RSF 24-12-00271) and the Ministry of Science and Higher Education, Russia: MICINN (PID2022-136297NB-IO0 /AEI/10.13039/501100011033/ FEDER, UE, PID2021-124050NB-C31, PID2019-104676GB-C33 PID2024-157541NB-IO0 (UAM) and PID2023-146401NB-IO0 (US). Severo Ochoa Centres of Excellence Programme 2025-2029 (CEX2024001442-S). Government of Andalucia (FQM160) and the University of Tokyo ICRR's Inter-University Research Program FY2025 Ref. J1, and ERDF and European Union (UAM: H2020-MSCA-RISE-GA872549- SK2HK) and NextGenerationEU funds (PRTR-C17.I1) and Generalitat de Catalunya (AGAUR 2021-SGR-01506, CERCA programme) University of Seville grant (RYC2022-035203-I funded by MICIU/ AEI/10.13039/501100011033, "ERDF a way of making Europe" and FSE+, Ayudas "Atracción de Investigadores con Alto Potencial". VII Plan Propio de Investigación y Transferencia, 2025 Ref. VIIPPIT-2023-V.4, and Secretariat for Universities and Research of the Ministry of Business and Knowledge of the Government of Catalonia and the European Social Fund (2022FI_B 00336), Spain; the SNSF and SERI, Switzerland; the STFC and UKRI, the UK; the DOE, the USA, including through the US-Japan Science and Technology Cooperation Program in HEP; and NAFOSTED (103.99-2023.144,IZVSZ2.203433), Vietnam. We also thank CERN for the UA1/ NOMAD magnet, DESY for the HERA-B magnet mover system, the BC DRI Group, Prairie DRI Group, ACENET, SciNet, and CalculQuebec consortia in the Digital Research Alliance of Canada, and GridPP in the UK, the CNRS/IN2P3 Computing Center in France and NERSC, the USA. Moreover, the participation of individual researchers and institutions has been further supported by funds from the ERC (FP7), 'la Caixa' Foundation, the Horizon 2020 Research and Innovation Programme of the European Union under the Marie Sklodowska-Curie grant; the JSPS, Japan; the Royal Society, the UK; the French ANR and Sorbonne Université Emergences programmes; the VAST-JSPS (no. QTJP01.02/20-22); and the DOE Early Career Program, the USA, For open access, we have applied for a Creative Commons Attribution (CC BY) license to any Author Accepted Manuscript version arising.

Author contributions The operation, Monte Carlo simulation and data analysis of the T2K and NOvA experiments are carried out by the T2K and NOvA Collaborations with contributions from all collaborators listed as authors on this paper. The scientific results presented here have been presented to and discussed by the full collaborations, and all authors have approved the final version of the paper.

Competing interests The authors declare no competing interests.

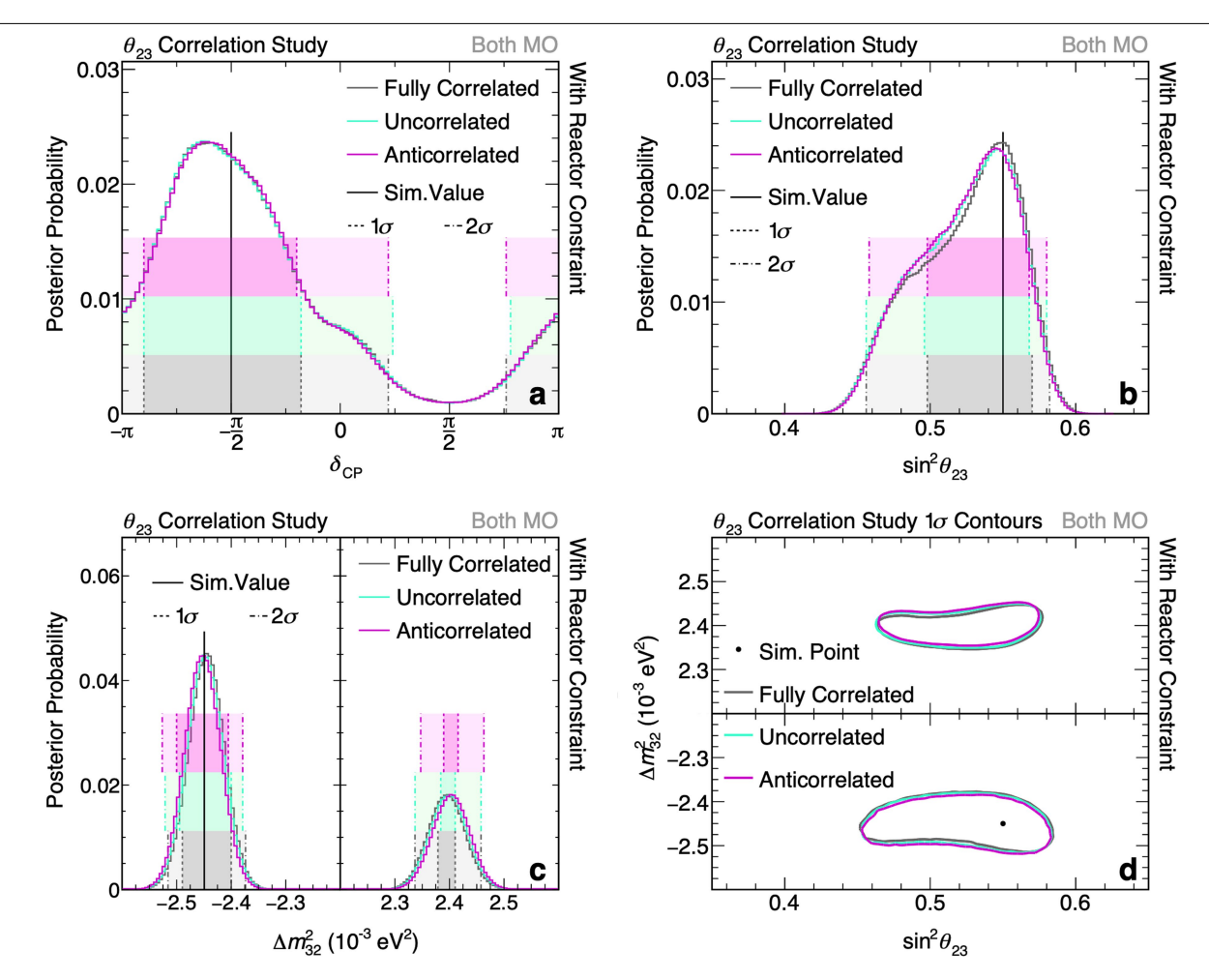
Additional information

Supplementary information The online version contains supplementary material available at https://doi.org/10.1038/s41586-025-09599-3.

Correspondence and requests for materials should be addressed to the NOvA Collaboration or the T2K Collaboration.

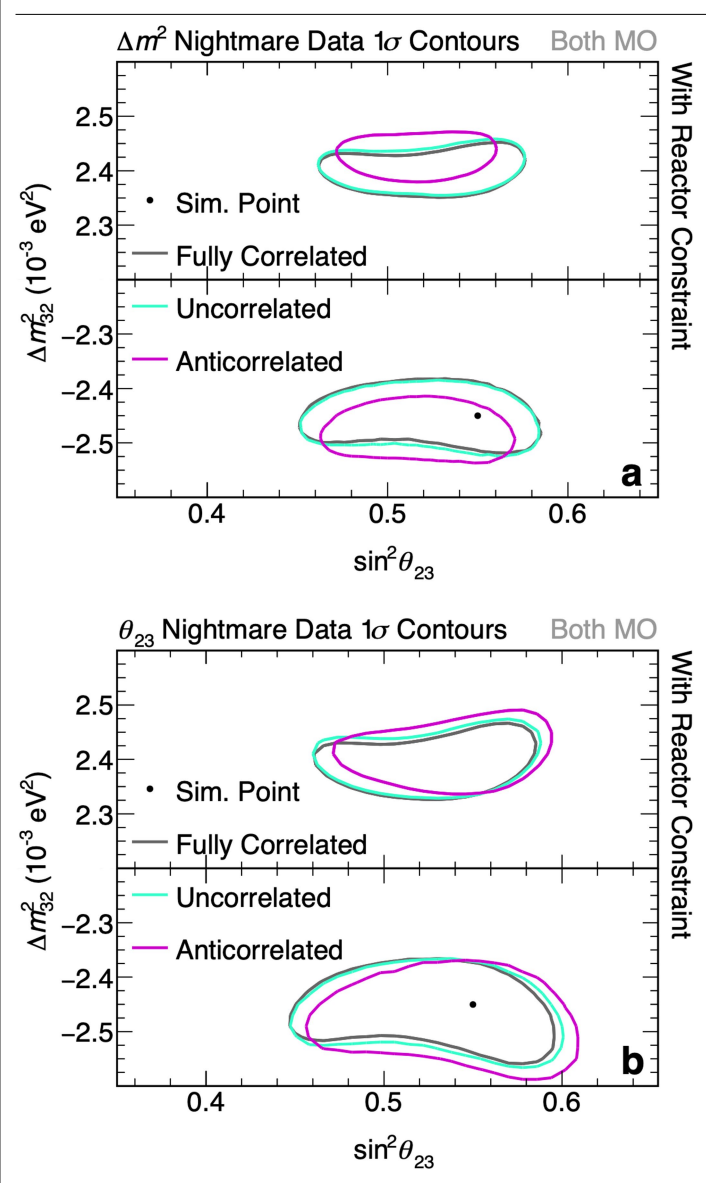
Peer review information Nature thanks Michele Lucente, Davide Meloni and Silvia Pascoli for their contribution to the peer review of this work. Peer reviewer reports are available.

Reprints and permissions information is available at http://www.nature.com/reprints.

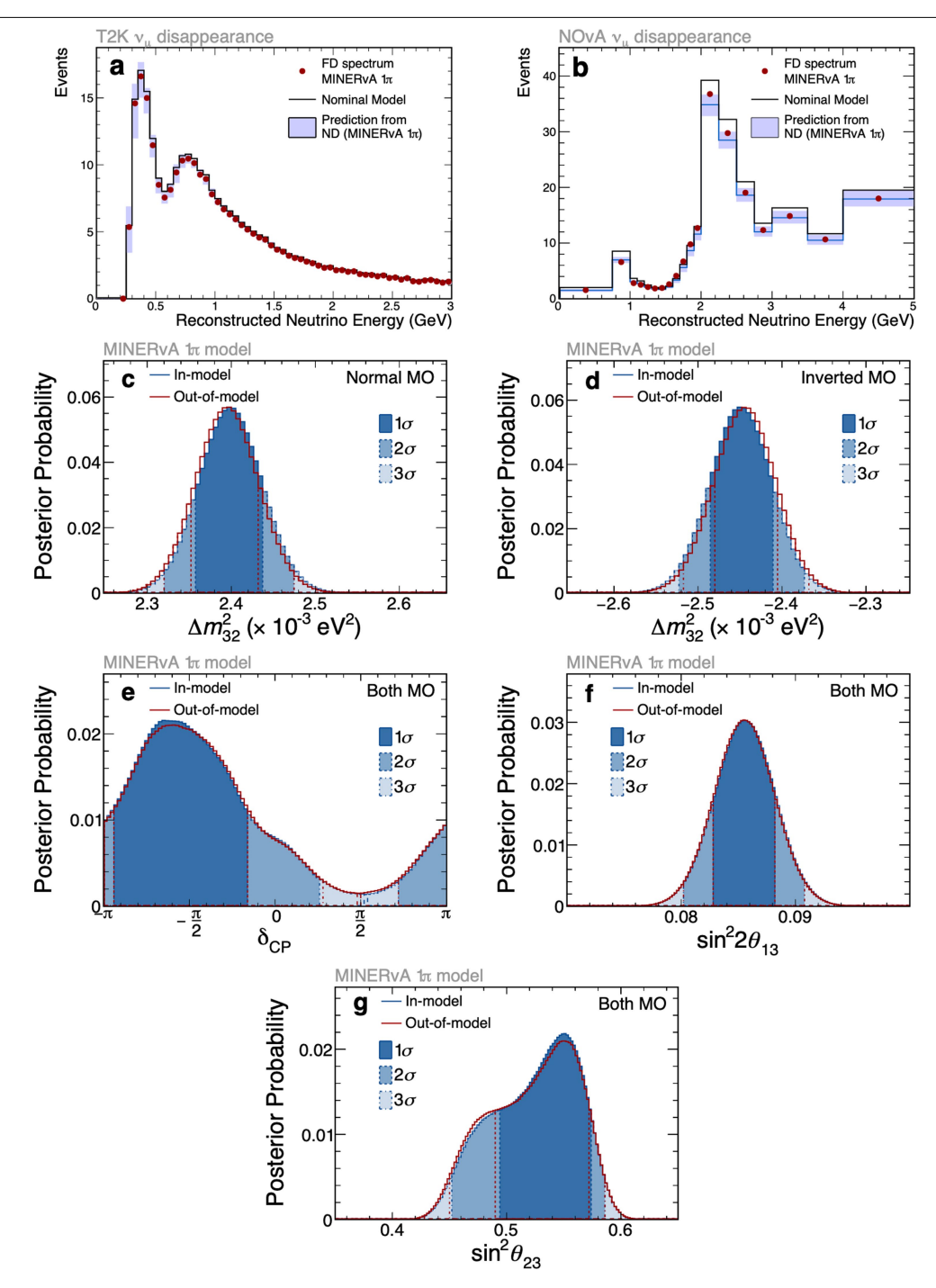


Extended Data Fig. 1| **Correlation study comparison plots.** Posterior probability distributions of $\delta_{\rm CP}$ (a), $\sin^2\theta_{23}$ (b), and Δm_{32}^2 (c) and 1σ credible regions in $\Delta m_{32}^2 - \sin^2\theta_{23}$ (d), marginalized over both neutrino mass ordering hypotheses ('Both MO') from fits to pseudo-data simulated with the NuFit-like oscillation parameter values. The fits were run in three configurations while

treating the systematic uncertainties with the largest impact on $\sin^2\theta_{23}$ (visible neutron energy and 2p2h C/O scale) as either 100% correlated (gray), uncorrelated (teal), or 100% anticorrelated (magenta). Overlaid with the corresponding 1σ (dark shaded areas, dashed) and 2σ (light shaded areas, dash-dotted) credible intervals.

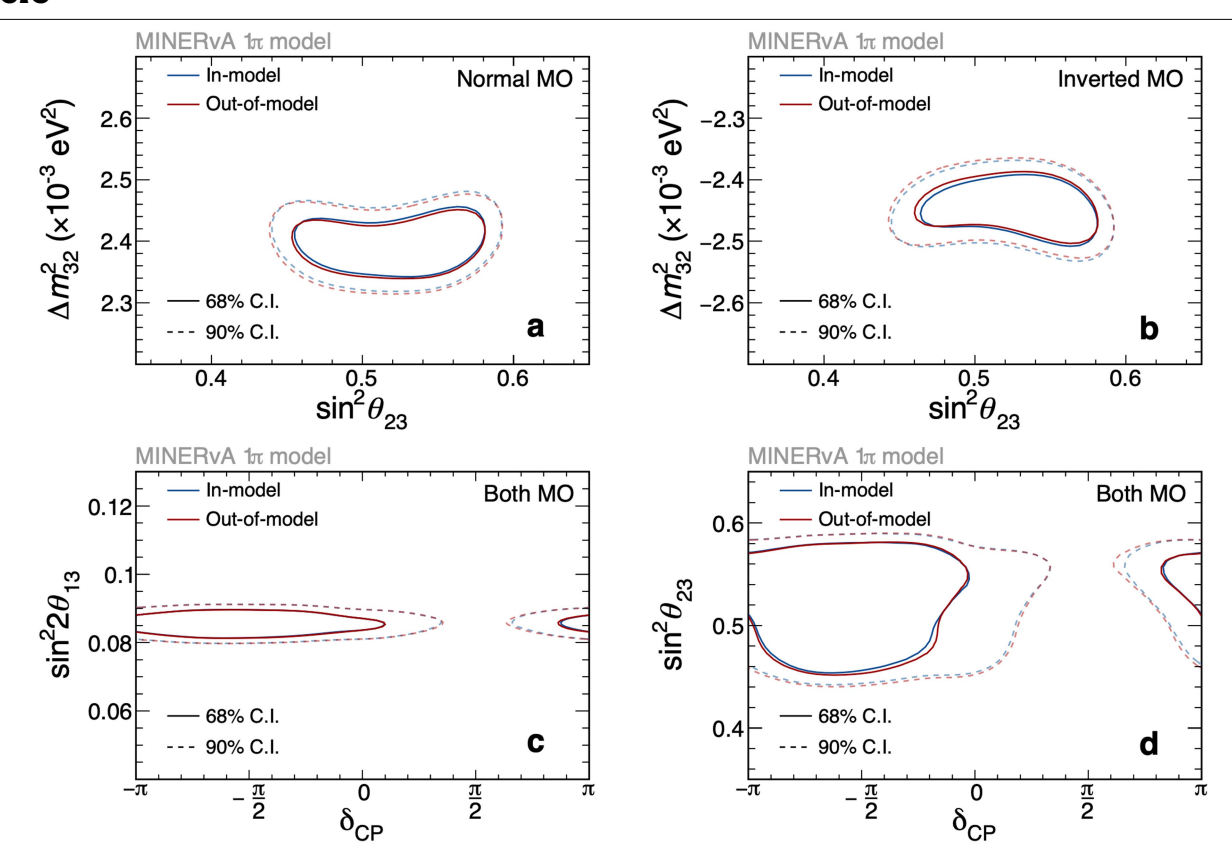


Extended Data Fig. 2| 'Nightmare' study comparisons. 1σ credible regions in $\Delta m_{32}^2 - \sin^2\theta_{23}$ posterior probability distributions marginalized over both neutrino mass ordering hypotheses ('Both MO') from fits to pseudo-data simulated with the NuFit-like oscillation parameter values and a fully symmetric systematic bias to affect (a) Δm_{32}^2 (' Δm^2 nightmare') and (b) $\sin^2\theta_{23}$ (' θ_{23} nightmare'). The fits were run while treating the NOvA and T2K nightmare parameters as either 100% correlated (gray), uncorrelated (teal), or 100% anticorrelated (magenta).



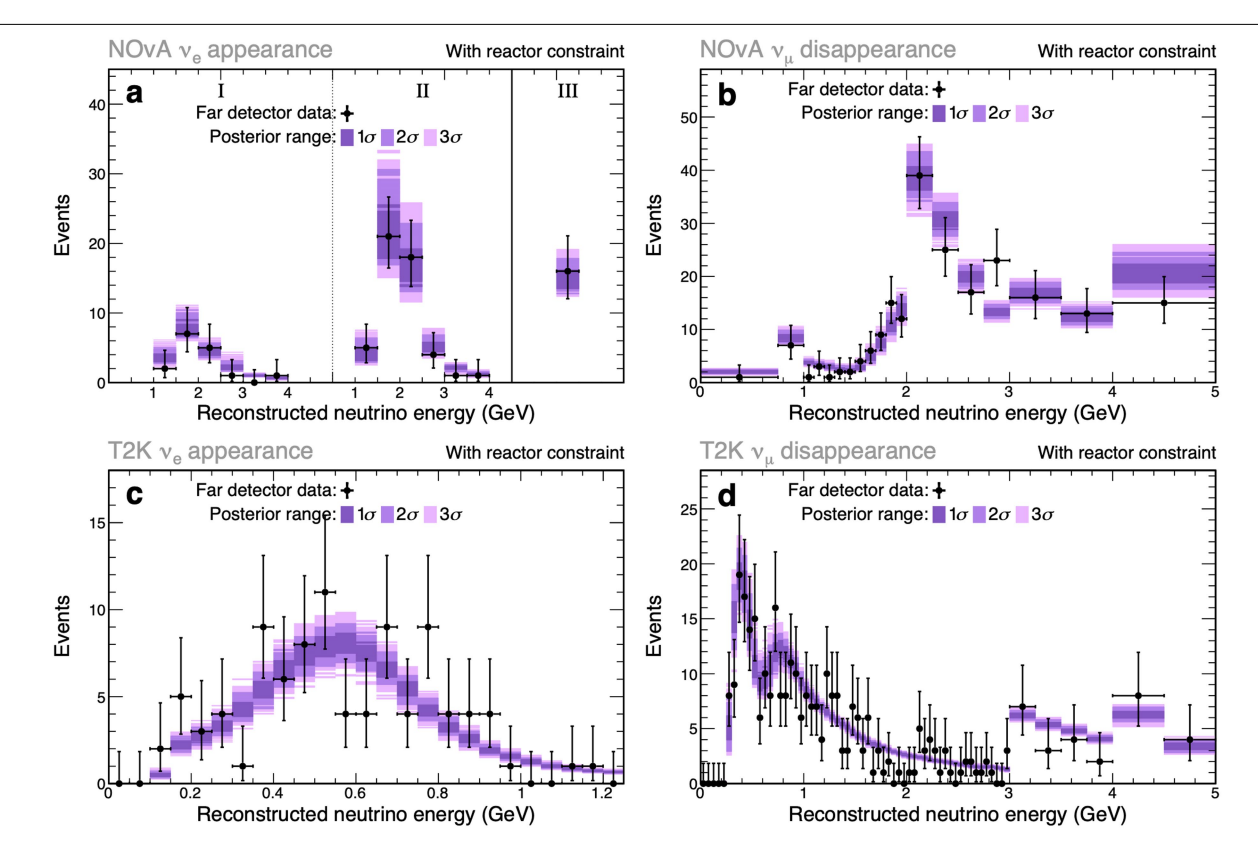
Extended Data Fig. 3 | **Out-of-model study spectra and comparison plots in 1D.** NOvA+T2K out-of-model study with suppressed pion production at low Q^2 ('MINERvA 1π ' case). The change on the FD pseudo-data and prediction with systematic uncertainties after incorporating the alternate data at the ND is shown for T2K (a) and NOvA (b). Central value of the nominal model is shown for comparison. 1D posterior probability distributions from a fit to pseudo-data

generated at the NuFit-like oscillation parameter values are shown for Δm_{32}^2 marginalized separately over the normal (c) and inverted (d) mass orderings, and for $\delta_{\rm CP}(e)$, $\sin^2 2\theta_{13}(f)$, and $\sin^2 \theta_{23}(g)$ marginalized over both mass orderings. The in-model (blue shaded) and out-of-model (red curve) scenarios are displayed.



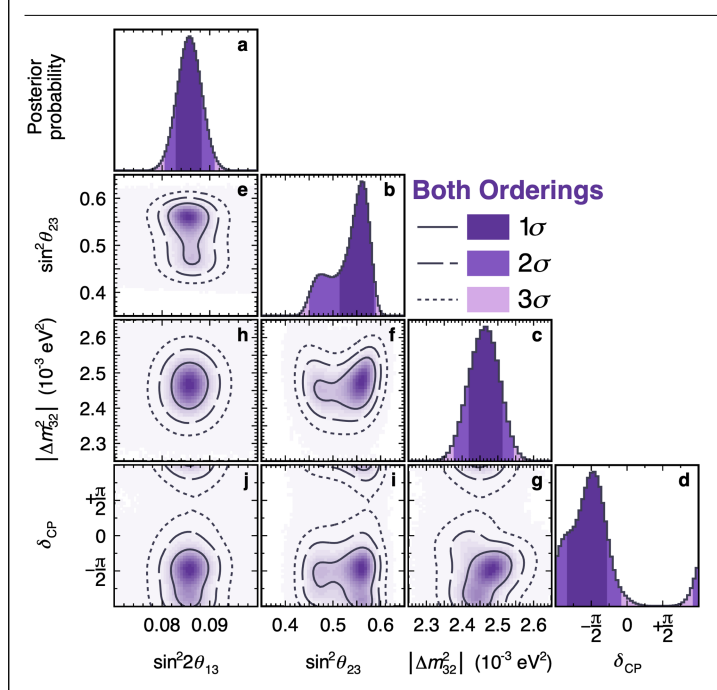
Extended Data Fig. 4 | **Out-of-model study comparison plots in 2D.** NOvA+T2K out-of-model study with suppressed pion production at low Q^2 ('MINERvA1 π ' case). 68% and 90% contours are shown on the $\sin^2\theta_{23} - \Delta m_{32}^2$ surface marginalized separately over the normal (a) and inverted (b) mass

orderings, and on the surfaces of δ_{CP} – $\sin^2 2\theta_{13}$ (c) and δ_{CP} – $\sin^2 \theta_{23}$ (d) parameters, marginalized over both mass orderings, from a fit to pseudo-data generated at the NuFit-like oscillation parameter values. The in-model (blue shaded) and out-of-model (red curve) scenarios are shown.

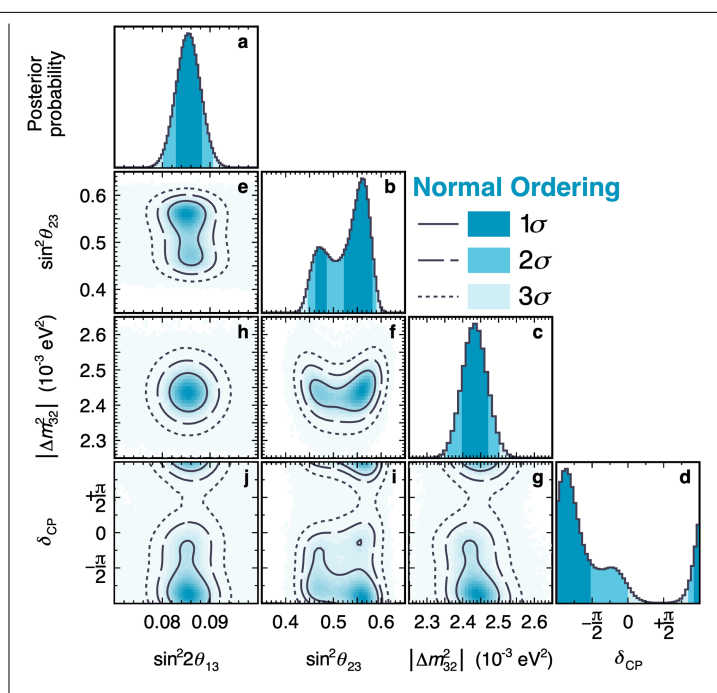


Extended Data Fig. 5 | **NOvA and T2K post-fit spectra.** NOvA (a, b) and T2K (c, d) posterior spectra compared to observed data for the largest ν_e -like (a, c) and ν_μ -like (b, d) event samples with the beam running enriched in ν_μ (as opposed to $\overline{\nu}_\mu$) extracted from a fit with reactor constraint, marginalized over both mass

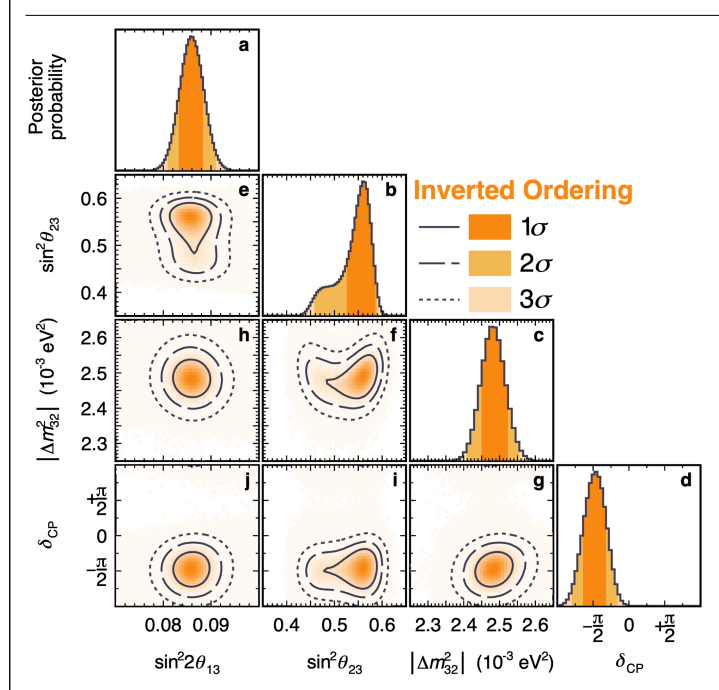
orderings. The NOvA ν_e -like sample (a) is divided into three subsets as shown here: events with a lower (I) or higher (II) event classification score and events lying near the periphery of the detector (III). Note that T2K also has a ν_e -like sample targeting events with single π not shown here.



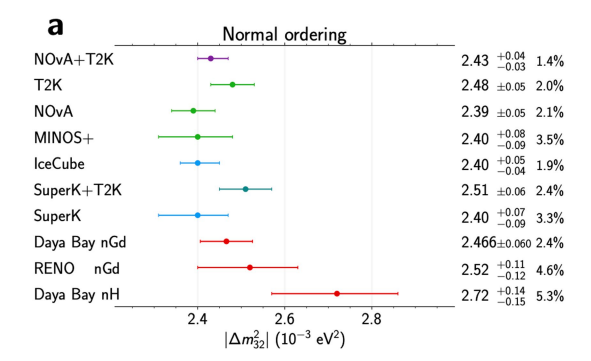
Extended Data Fig. 6 | **Constraints on PMNS oscillation parameters in 1D and 2D for both orderings.** The 1D posterior probability distributions of $\sin^2 2\theta_{13} \text{ (a)}, \sin^2 \theta_{23} \text{ (b)}, \left| \Delta m_{32}^2 \right| \text{ (c)}, \delta_{CP} \text{ (d)}, \text{ and corresponding } 1\sigma, 2\sigma, 3\sigma 2D \text{ contours } \sin^2 \theta_{23} - \sin^2 2\theta_{13} \text{ (e)}, \Delta m_{32}^2 - \sin^2 \theta_{23} \text{ (f)}, \delta_{CP} - \Delta m_{32}^2 \text{ (g)}, \Delta m_{32}^2 - \sin^2 2\theta_{13} \text{ (h)}, \delta_{CP} - \sin^2 \theta_{23} \text{ (i)}, \text{ and } \delta_{CP} - \sin^2 2\theta_{13} \text{ (j)} \text{ from the joint fit with reactor constraints marginalized over both mass orderings.}$

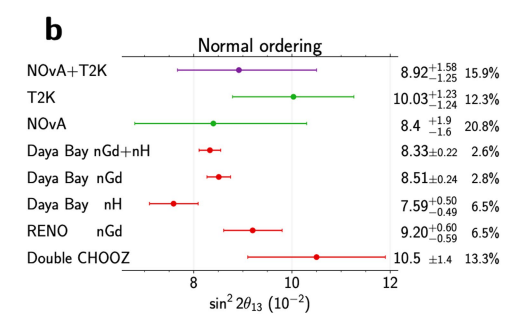


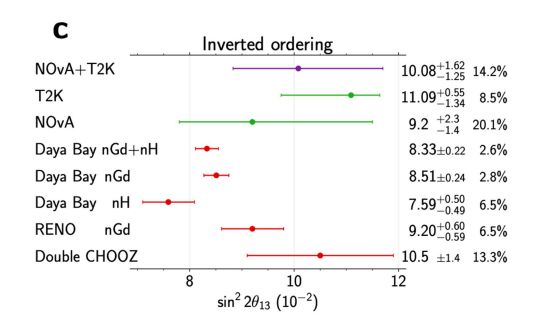
 $\textbf{Extended Data Fig. 7} | \textbf{Constraints on PMNS oscillation parameters in 1D} \\ \textbf{and 2D for normal ordering.} \\ As in Extended Data Fig. 6, but conditional on the assumption of normal ordering.}$



 $\label{lem:extended} \textbf{Extended Data Fig. 8} | \textbf{Constraints on PMNS oscillation parameters in 1D} \\ \textbf{and 2D for inverted ordering.} \\ \textbf{As in Extended Data Fig. 6}, but conditional on the assumption of inverted ordering.} \\$

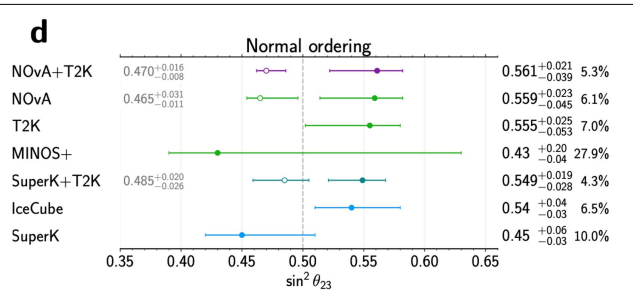


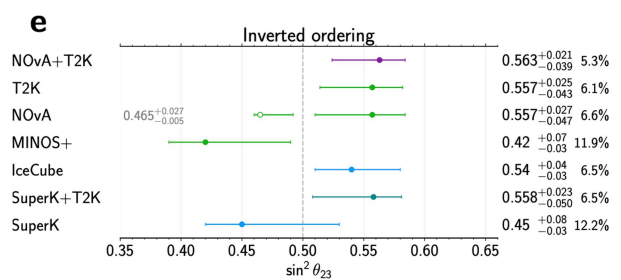


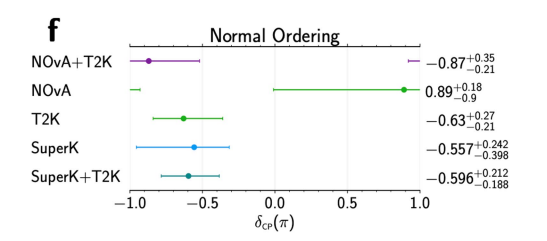


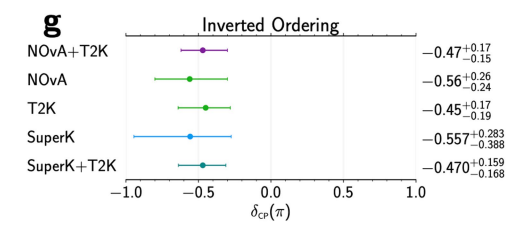
$Extended \, Data \, Fig. \, 9 \, | \, Experimental \, measurements \, of oscillation \, parameters.$

 $|\Delta m_{32}^2|$ assuming normal ordering (a), with sources for the results from top to bottom starting with the second line as follows: $^{13,14,43-49}$, $\sin^2 2\theta_{13}$ assuming normal (b) and inverted (c) ordering, with sources for the results from top to bottom starting with the second line as follows: $^{13,14,47-49,63}$. NOVA+T2K measurement here does not use the reactor constraint. $\sin^2 \theta_{33}$ assuming









normal (d) and inverted (e) ordering, with sources for the results from top to bottom starting with the second line as follows: $^{13,14,43-46}$. Open circles denote a local minima position in lower octant. $\delta_{\rm CP}$ assuming normal (f) and inverted (g) ordering, with sources for the results from top to bottom starting with the second line as follows: 13,14,45,46 .

Extended Data Table 1 | Default oscillation parameters for simulation

	T2K-like	NOvA-like	NuFit-like
$\Delta m_{32}^{2} \; (\text{eV}^{2})$	2.51×10^{-3}	2.41×10^{-3}	-2.45×10^{-3}
$\sin^2 \theta_{23}$	0.528	0.570	0.550
δ_{CP}	-0.51π	0.83π	-0.50π

Sets of oscillation parameter values used to generate pseudo-data. For all sets, $\sin^2\theta_{13}$ is 2.18×10^{-2} , Δm_{21}^2 is 7.53×10^{-5} eV², and $\sin^2\theta_{12}$ is 0.307.

Extended Data Table 2 | Posterior predictive p-values

	Rate + Shape										
						Subsamples <i>p</i> -value					
Channel	Joint <i>p</i> -value			$NOvA^a$			T2K ^{<i>b</i>}				
	Both	NO	Ю	Both	NO	Ю	Both	NO	10		
c	0.62	0.62 0.53	0.69	0.90	0.83	0.95	0.19	0.18	$0.20^{(u_{ m e})}$		
$ u_{e}{}^c$	0.02	0.55				0.95	0.79	0.78	$0.79^{(\nu_\mathrm{e}1\pi)}$		
$ar{ u}_{e}$	0.40	0.38	0.42	0.21	0.18	0.24	0.67	0.67	0.67		
$ u_{\mu}$	0.62	0.62	0.62	0.68	0.65	0.70	0.48	0.50	0.47		
$\overline{ u}_{\mu}$ $ar{\overline{ u}}_{\mu}$	0.72	0.73	0.71	0.38	0.38	0.37	0.87	0.87	0.87		
Total	0.75	0.73	0.76	0.64	0.60	0.68	0.72	0.73	0.71		
	Rate										

				Subsamples <i>p</i> -value					
Channel	Joint <i>p</i> -value		NOvA			T2K			
	Both	NO	10	Both	NO	Ю	Both	NO	IO
$\phantom{aaaaaaaaaaaaaaaaaaaaaaaaaaaaaaaaaaa$	0.40	0.14	0.57	0.48	0.16	0.71	0.39	0.43	$0.36^{(u_{ m e})}$
							0.11	0.12	$0.11^{(u_{ m e}1\pi)}$
$ar{ u}_{e}$	0.33	0.31	0.34	0.55	0.42	0.64	0.57	0.60	0.55
$ u_{\mu}$	0.15	0.17	0.14	0.24	0.23	0.25	0.11	0.10	0.12
$ar{ u}_{\mu}$	0.93	0.94	0.93	0.90	0.89	0.90	0.72	0.72	0.72
Total	0.40	0.28	0.49	0.58	0.39	0.70	0.24	0.27	0.22

Posterior predictive *p*-values extracted from the joint fits, marginalized over both mass orderings, normal mass ordering and inverted mass ordering with the reactor constraint. a NOvA: NOvA sample by sample from the joint fit.

b T2K: T2K sample by sample from the joint fit, v_e and v_e 1 π samples treated independently. c Joint: v_e channel p-value includes T2K v_e , T2K v_e 1 π and NOvA v_e .

Extended Data Table 3 | NOvA+T2K measurements of oscillation parameters

Parameter	Normal Ordering	Inverted Ordering		
$ \Delta m_{32}^2 $	$2.43^{+0.04}_{-0.03}$	$2.48^{+0.04}_{-0.03}$		
$\sin^2\! heta_{23}$	$0.561^{+0.021}_{-0.039}$ and $0.470^{+0.016a}_{-0.008}$	$0.563^{+0.021}_{-0.039}$		
δ_{CP}	$-0.87\pi^{+0.35\pi}_{-0.21\pi}$	$-0.47\pi^{+0.17\pi}_{-0.15\pi}$		
$\sin^2 2\theta_{13}$	0.0855 ± 0.0027	$0.0859^{+0.0027}_{-0.0025}$		

Values assume normal and inverted ordering with the reactor constraint applied. a Local extremum in lower octant of $\sin^2\!\theta_{23}$.